Loughborough University

MASTER'S THESIS

# Computer Modelling of Turbulence Premixed Combustion Relevant to SI Engines

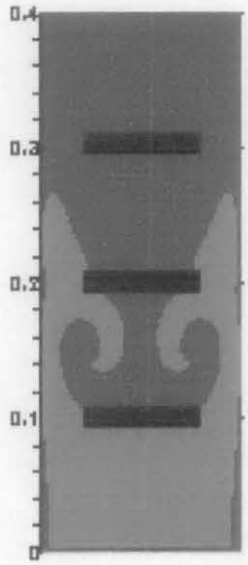


**Mohd Arief**

**MSc in Automotive Systems Engineering**
**Department of Aeronautical & Automotive Engineering**
**Loughborough University**

# Summary

The identification on the nature of Spark Ignition (SI) engine combustion shows that the engine flames can be classified as turbulence premixed type. It consists of complex phenomena such as reaction, diffusion, volume expansion and in general involves complicated geometries, complex physics, heat transfer, and fluid flow. Because of the above factors, the need of models to simulate these combustion processes is highly demanded to evaluate the performance of different designs, perform parametric studies and virtual prototype each design before actual fabrication.

Computer simulations were carried out using an in-house RANS CFD code being developed at Loughborough University, known as Turbulence Reactance Flow 2-Dimension (TRF2D), to evaluate its capability whether it will be suitable to be applied for the simulation of SI engine. Since the code is still in the development stage, comparison of its capability were asessed with experimental results that use mounted obstacles to allow the build-up of turbulence creating complex interaction and challenging problem for numerical model. Results were discussed based on the structure of flame propagation, flame location and the pressure time history within the combustion chamber. The identification of the approach applied were also discovered based on its combustion regimes.

A comprehensive study of the modelling technique used in TRF2D was carried out and improvements needed for standard k-ε turbulence model and the non-linear k-ε turbulence model were identified. In general, by using a standard turbulence model, the code failed to reproduce the recirculation phenomena that took place in the combustion chamber. Meanwhile, the modified non-linear turbulence model has shown a good correlation with the experimental results. The code has also shown its capability in simulating various different fuel mixtures.

The identification of the approach has summarised that TRF2D is best suited for the studies of SI engine combustion as the calculated results by the model were found to be in the region of the SI engine reaction.

# Acknowledgements

I extend my sincere gratitude and appreciation to a number of people who made this master thesis possible.

I am indebted to my supervisor Dr Salah Ibrahim for his encouragement, guidance and invaluable CFD expertise.

I would also like to acknowledge with appreciation the help, support and constructive comments of Dr. Mohamed Yehia, a visiting lecturer from the University of Cairo, Egypt.

Many thanks to the head of the Automotive Department Prof. Tim Gordon for his support.

Finally, I feel especially indebted to Barbara Jibson and Anoma Malalasekera, though they have no direct relation with my research, but they have given me much assistance and help throughout the course.

# Nomenclature

**Latin Symbols**

| | |
|---|---|
| $a, b, c..$ | Consumption reaction rate orders |
| $A_s$ | Species concentration |
| $A, B, C..$ | Reactant species |
| $c$ | Reaction progress variable |
| $C_L$ | BML model constant |
| $c_d$ | Integral length scale constant |
| $D$ | Fractal dimension |
| $Da$ | Dimensionless Damkohler number |
| $D_L$ | Laminar fractal dimension |
| $D_T$ | Turbulent fractal dimension |
| $e$ | Specific internal energy ($Jkg^{-1}$) |
| $g$ | BML reaction rate parameter |
| $k$ | Turbulence kinetic energy ($m^2s^{-2}$) |
| $k_f$ | Reaction rate for coefficient for forward reaction |
| $k_r$ | Reaction rate coefficient for reverse reaction |
| $K$ | Dimensionless Karlovitz number |
| $l$ | Integral length scale |
| $l_F$ | Flame thickness |
| $L$ | Length scale |
| $L_y$ | Wrinkling length scale (m) |
| $P$ | Pressure ($Nm^{-2}$) |
| $R$ | Mean rate of chemical reaction per unit area ($kgm^{-2}s^{-1}$) |
| $R_L$ | Turbulent Reynolds number |
| $Re$ | Dimensionless Reynolds number |
| $R_o$ | Universal gas constant ($Nmkmol^{-1}K^{-1}$) |
| $S$ | Number of different species |
| $S$ | Flow strain ($s^{-1}$) |
| $S_L$ | Flame speed ($ms^{-1}$) |
| $t$ | Time (s) |
| $t_F$ | Flame time |
| $t_T$ | Turbulent time |
| $t_\eta$ | Kolmogorov time |
| $T$ | Temperature (K) |
| $T_s$ | Turbulent flow stretch term ($m^{-1}s^{-1}$) |
| $u$ | Axial flow velocity ($ms^{-1}$) |
| $u_L$ | Laminar burning velocity ($ms^{-1}$) |
| $\nu_{rs}$ | Stoichiometric coefficient of reactance |
| $W$ | Rate of chemical reaction ($kgm^{-3}s^{-1}$) |

**Greek Symbols**

| | |
|---|---|
| $\alpha$ | Parameter in the $T_s$ term |
| $\beta$ | Parameter used to calculate $u_L$ |
| $\delta_L$ | Laminar flame thickness (m) |
| $\varepsilon$ | Rate of dissipation of $k$ ($m^2s^{-3}$) |
| $\Delta H$ | Change in specific enthalpy ($Jkg^{-1}$) |
| $\sigma$ | Prandtl/Schmidt number |
| $\sigma_y$ | BML reaction rate parameter |
| $\phi$ | Arbitrary variable |
| $\eta$ | Kolmogorov microscale (m) |
| $\lambda$ | Thermal Conductivity ($Wm^{-1}K^{-1}$) |
| $\mu_T$ | Turbulent eddy viscosity |
| $\nu$ | Kinematic viscosity |
| $\Omega$ | Vorticity |
| $\rho$ | Density |
| $\rho_u$ | Density of unburnt mixture |
| $\rho_b$ | Density of burnt mixture |
| $\tau$ | Heat release parameter |
| $\tau_{ij}$ | viscous stress tensor ($Nm^{-2}$) |

**Others**

| | |
|---|---|
| - | Reynolds averaged mean value |
| ~ | Favre averaged mean value |
| ' | Difference from Reynolds averaged mean value |
| '' | Difference from Favre averaged mean value |

# Table of Contents

# 1 Introduction

Combustion is of great importance in modern society, as a means of supplying energy for everyday use, for powering vehicles, and for industrial processes. Turbulent Combustion occurs frequently in Internal Combustion (IC) engines, gas turbines, furnaces etc. Premixed Combustion - in which the fuel and oxidant are thoroughly mixed before combustion - is a special limiting case (Turns, 2000).

In combustion processes, fuel and oxidizer (typically air) are mixed and burned. It is useful to identify several combustion categories based upon whether the fuel and oxidizer are mixed first and burned later (*premixed*) or whether combustion and mixing occur simultaneously (*nonpremixed*). Each of these categories is further subdivided based on whether the fluid flow is laminar or turbulent. Table 1 shows examples of combustion systems that belong to each of these categories, which will be discussed in the following sections.

**Laminar Premixed Flames:** In laminar premixed flames, fuel and oxidizer are premixed before combustion and the flow is laminar. Examples are laminar *flat flames* and (under fuel-lean conditions) *Bunsen flames* (see figure 1.1)

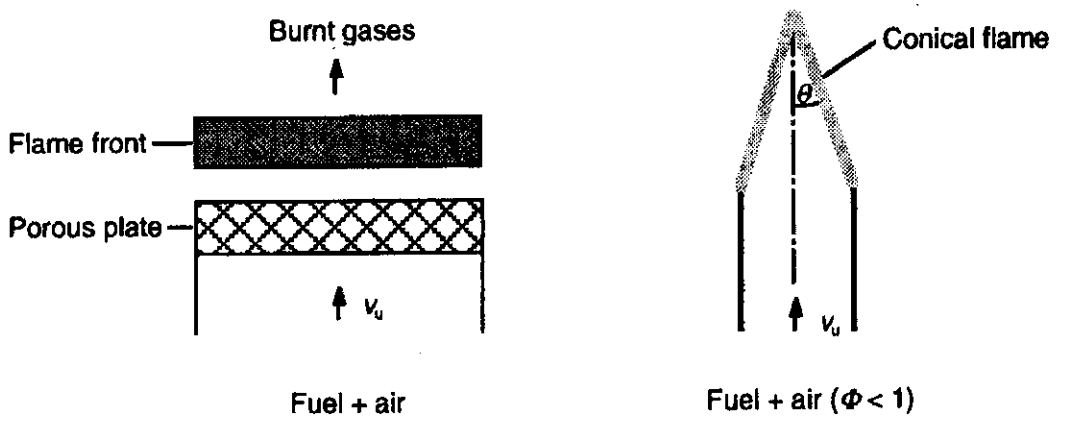


**Figure 1.1. Schematic illustration of a laminar flat flame (left) and of a Bunsen flame (right), both premixed (Warnatz, 1996)**

**Turbulent Premixed Flames:** As Table 1 indicates, other examples of premixed flames include the ubiquitous spark-ignited engine (Otto engine) where the flow is seldom laminar. In this case, premixed flame fronts burn and propagate into a turbulent fluid flow. If the turbulence intensity is not too high, curved laminar premixed flame fronts are formed. The turbulent flame can then be viewed as an ensemble of many premixed laminar flames.

**Table 1. Example of combustion systems ordered with respect to premixedness and flow type**

| Fuel/Oxidizer Mixing | Fluid Motion | Examples |
|---|---|---|
| **Premixed** | Turbulent | Spark-ignited gasoline engine |
| | | Low $NO_x$ stationary gas turbine |
| | Laminar | Flat flame |
| | | Bunsen flame |
| **Non-premixed** | Turbulent | Pulverized coal combustion |
| | | Aircraft turbine |
| | | Diesel engine |
| | | $H_2/O_2$ rocket motor |
| | Laminar | Wood fire |
| | | Radiant burners for heating |
| | | Candle |

Nowadays almost all vehicles use the internal combustion engine, of the reciprocating type. In this the combustion gases are the working fluid that drives the mechanical power delivery. The birth of this engine, as commercial proposition, was in 1860 with the Lenoir spark ignited gas engine. The cycle operated at atmospheric pressure, therefore being severely limited in power output capability. In 1876 was demonstrated the basis for the vehicle engine in use today, with the major advancement conceived by Otto that greater power could result by raising the pressure of the working fluid before adding the energy to it through combustion. These early *compression* engines, as they were known, were limited to stationary applications, due to the need for connection to a gas supply (usually town gas, from the retorting of coal, the only "fluid" fuel then generally available). This is where the influence of the availability of petroleum, providing a source of liquid fuels with high energy density, both accelerated and started to govern developments, resulting in the engine types we see today. From this era the evolution of fuels and vehicle

engines has been closely intertwined, with the combination inseparable when considering the resulting emissions performance characteristics.

Before looking at the specifics of combustion in the Internal Combustion (IC) engine, it is useful to prepare the ground with some simple introduction to the basic generics of the combustion process itself. Any substances that unite with the evolution of heat can be regarded as a "fuel", but here we consider the commonly recognised combustion process, involving a hydrocarbon fuel such as petroleum products.

Combustion is the thermo-chemical reaction process between the oxygen in air and the hydrocarbon fuel, to form the theoretical products of $CO_2$ and $H_2O$, with the attendant release of heat. The actual reaction occurs in the gas phase, so the fuel medium must be gasified before it can take part in the process, mixed with oxygen (air) and then provided with the energy of ignition for the self-sustaining chemical reaction to proceed. The obvious desire is for complete combustion, that is 100% conversion of reactants to products and full heat release, but this requires perfect control of the process such that the fuel is completely gasified, mixed with the correct amount of air (the stoichiometric ratio), presented to the ignition zone and allowed to react completely without premature quenching of the flame. Any shortcomings in this will lead to imperfect combustion, with the natural consequence being the release of other than $CO_2$ and $H_2O$, or "emission" as we know them.

As combustion reactions are exothermic the heat energy evolved maintains the reaction temperature, thereby initiating succeeding oxidation, but there has to be an initiation for the process; a fire needs to be lit, and in the petrol engine there needs to be a spark in each cycle. This first ignition needs to be provided at the right time and place throughout the fuel: air mix, before flame front ignition takes over, and at this point is where the important distinction between "premixed' and "diffusion" burning. When and how the fuel and air are introduced to the combustion zone determines which general mechanism is dominant. Premixed, as the term suggests, has the fuel in the gas phase, intimately and homogeneously mixed with the air, ready to undergo combustion. In a steady state combustion system this mixture is then fed continually to the combustion zone, the flame providing the energy for ignition. Conversely, in

batch type, or cyclical combustion, the mixture is contained in a combustion chamber, then ignited initially from a central point and the flame front progresses through the flammable mixture. The most notable example of the latter is the spark ignited petrol engine. Figure 1.2 below, shows an example of a four stroke spark ignition engine, which are commonly used in automotive industry.

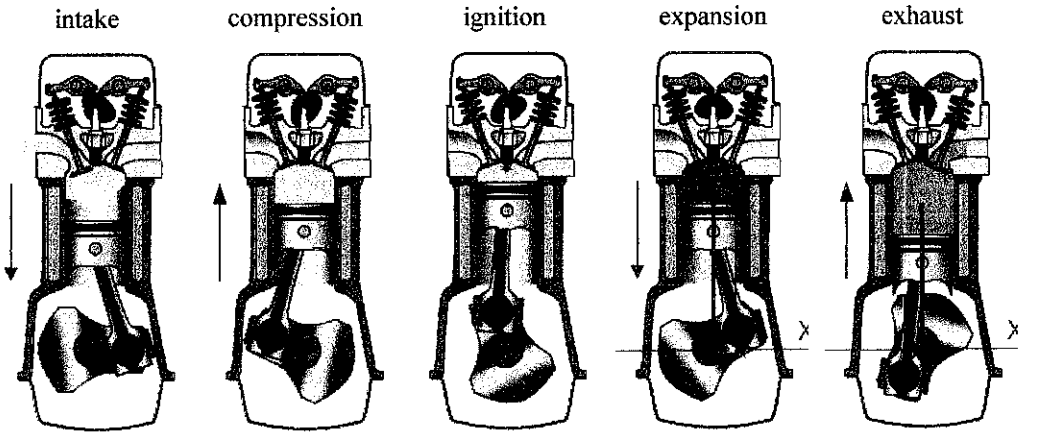


**Figure 1.2. The cycle of a 4 stroke SI engine (the arrows indicates the direction of the piston movement)**

The simplified sequence of events in the SI cycle are as follows; Fuel is metered by the carburetor or fuel injection system into the induction air, maintaining essentially constant air fuel ratio (AFR) throughout the load/power range as controlled by the throttle. Fuel evaporation and mixing is ideally complete before the mixture enters the cylinder, such that the charge is fully prepared prior to the compression stroke.

As the piston approaches top-dead-centre (TDC), the timed spark ignites the compressed mixture, the location of the spark plug in conjunction with the geometry of the combustion chamber providing for the ordered propagation of the flame front through the mixture. Spark timing is optimised against the design, compression ratio and anti-knock quality of the petrol fuel, over the range of engine speed and load (i.e. power) demand. The motion of the charge through the induction and compression strokes needs also to generate turbulence in the mixture to speed the flame propagation, for combustion to be completed in the time available before the exhaust phase; the induced micro-turbulence breaks up the flame front, giving more surface area for the reaction process.

In general, the studies of turbulent premixed flames are important because of their occurrence in spark ignition engines as mentioned by Maly, 1994. Their behaviour is difficult to describe since several inter-connected processes - reaction, diffusion, volume expansion - occur in inhomogeneous flows. Because of these concerns, the need of models to simulate these combustion processes is highly demanded. While existing theoretical models have already been found to be useful in all of these applications discerning users find inevitable shortcomings in their performance.

# 2 Computational Fluid Dynamics (CFD)

It is well known that the reciprocating engines exhibit many complex features and phenomena, perhaps more complex than any other mechanical device. Although the SI engine has gone through over a century of very ambitious development, the margin for improvement can still be considered as relatively wide. Regulations, economy and emissions targets, new technologies, development time and cost reduction and marketing constraints require engineers to develop and propose increasingly sophisticated solutions in order to improve performance even further. To cope with the demands, control over combustion is a key objective, but one that is difficult to attain due to the complexity of the processes involved. Basically, these processes include the flow of air and the fuel into the combustion chamber, mixing of air and fuel, ignition, combustion and thus formation of exhaust gases. Reduction of engine emissions and fuel consumption can be reached by an improved control over the degree of homogeneity of the air-fuel mixture, cycle-to- cycle variation, and turbulence intensity as well as large- scale motion.

As been discussed earlier in chapter 1, combustion problems in SI engine generally involve complicated geometries, complex physics, heat transfer, and fluid flow. In such a challenging environment, the benefits from CFD modelling cannot be overstated. Since combustion systems are extremely costly to build and test, CFD can be a valuable tool to model the performance of different designs, perform parametric studies and virtual prototype each design before actual fabrication.

The work is then aimed at improving the understanding of the processes involved, and providing models, which can be used as design tools. In particular, the wish to improve the computer modelling of combusting flows. These computer models can be used to:

- aid understanding
- improve efficiency
- reduce hazardous emission
- reduce design costs and development times

## 2.1 Overview of CFD

Computational Fluid Dynamics (CFD) has grown from a mathematical curiosity to become an essential tool in almost every branch of fluid dynamics, from aerospace propulsion to weather prediction. CFD is commonly accepted as referring to the broad topic encompassing the numerical solution, by computational methods, of the governing equations which describe fluid flow, the set of the Navier-Stokes equations, continuity and any additional conservation equations, for example energy or species concentrations.

As a developing science, Computational Fluid Dynamics has received extensive attention throughout the international community since the advent of the digital computer. There are two main attractions to the subject. Firstly, the desire to be able to model physical fluid phenomena that cannot be easily simulated or measured with a physical experiment, for example weather systems or hypersonic aerospace vehicles. Secondly, the desire to be able to investigate physical fluid systems more cost effectively and more rapidly than with experimental procedures.

There has been considerable growth in the development and application of Computational Fluid Dynamics to all aspects of fluid dynamics. In design and development, CFD programs are now considered to be standard numerical tools, widely utilised within industry. As a consequence there is a considerable demand for specialists in the subject, to apply and develop CFD methods throughout engineering companies and research organisations.

## 2.2 Weaknesses of the combustion modelling

The limitations of models in present CFD explosion codes and the challenges in development of new models are related to broadening the validity of turbulent burning velocity models. A range of turbulent burning data exists for methane and propane mixtures, but data are rare for most other fuel mixtures. Very few turbulent burning velocity data from experiments exists at elevated pressure or in turbulence

fields with high intensity or large length scale. The burning velocity model used in explosion calculations is therefore to a large degree based only on extrapolation of data. More experimental burning data is needed to improve the turbulent burning velocity model used in explosion codes.

The turbulent flow field in a SI engine includes many complicated features, such as swirl, recirculation and combustion, and to develop it, usually both numerical simulations and experiments are required. However, in numerical simulations, standard models fail in the prediction of swirling flows and it is well known that different turbulence models capture the swirling motion with different levels of accuracy.

Recent advances in computational power have meant that the application of CFD is now quite common. Many such simulations use the k-ε turbulence model to represent turbulent transport. In this approach the Reynolds stress is linearly related to the mean rate of strain via an eddy viscosity, and while it is often capable of providing good results, it does have serious limitations. It is incapable of reproducing, for example swirling motions and the effects of strong streamline curvature. Therefore, a more detailed description of turbulent transport is required.

Currently the only tractable approach to the modelling of turbulent combusting flows is that based on closures through the use of Favre or density-weighted averaging of the conservation equations. However, the averaging process results in more unknowns than equations. In combusting flows these unknowns are of two types, the density-weighted Reynolds stress and turbulent scalar flux – the second moments. For turbulent transport, second moment closures represent an optimum choice, they combine a reasonably detailed turbulence representation at an acceptable level of complexity. With such approaches all the second moments are obtained from the solution of modelled partial differential equations. The modelled equations are obtained through approximations to relate higher order unknown correlations to lower order known quantities.

# 3 Turbulence

There are three possible flow situations; laminar, transitional and turbulent. Laminar flows are smooth and structured; transitional flows occur when laminar flow becomes turbulent. Turbulent flows seem irregular, chaotic and unpredictable and are characterised by a rapid rate of diffusion of momentum and heat. Most flows in engineering problems are turbulent. In 1883 Osborne Reynolds performed experiments on pipe flow (shown in Kundu, 1990). This was the first systematic work on turbulence, and he found that the flow becomes turbulent when the non-dimensional ratio exceeds a certain value. The ratio is called Reynolds number

$$\mathrm{Re} = \frac{UL}{\nu} \tag{3-1}$$

where, $U$ is the velocity, $L$ is the length scale (here, the diameter of the pipe) and $\nu$ is the kinematic viscosity. Turbulence occurs at high Reynolds numbers and it consists of random fluctuations in both space and time. It should be noted that turbulence is a property of the flow and not of the fluid.

## 3.1 Flame Types

There are basically two types of flames; premixed flames or non-premixed (diffusion) flames as been discussed earlier in Chapter 1. In a premixed flame, the fuel and the oxidiser are mixed before any significant chemical reaction occurs. In a diffusion flame, the reaction occurs only at the interface between the fuel and the oxidiser, where mixing and reaction both take place. Both types of flames can be either laminar or turbulent. Only turbulent premixed flames will be discussed here.

An important factor in the understanding of turbulent combustion is the different time and length scale ratios. The interaction between chemistry and turbulence can be classified by two criteria: premixed or non-premixed combustion, slow or fast

chemistry. Slow chemistry has few practical applications and this implies that fast chemistry occurs in nearly all situations. To have stable combustion it must be rapid and all chemical time scales associated with the process must be small. If Favre-averaged (discussed later in chapter 6.2) quantities are used, the integral length scale can be expressed (Libby et al, 1994) as

$$l = \frac{c_d u'^3}{\tilde{\varepsilon}} \tag{3-2}$$

where $c_d$ is a constant and $u'$ is the velocity fluctuation. With the integral length scale it is possible to express the turbulent time

$$t_T = \frac{l}{u'} \tag{3-3}$$

The Kolmogorov length and time scales expressed in Favre-averaged quantities are

$$\eta = \left(\frac{\nu^3}{\tilde{\varepsilon}}\right)^{\frac{1}{4}} \tag{3-3}$$

$$t_\eta = \left(\frac{\nu}{\tilde{\varepsilon}}\right)^{\frac{1}{2}} \tag{3-4}$$

As an intermediate scale, the Taylor length scale

$$\lambda = \left(\frac{\nu u'^2}{\tilde{\varepsilon}}\right)^{\frac{1}{2}} \tag{3-5}$$

may also be considered. Defined the Damkholer number as the ratio of the turbulent time to the flame time

$$Da = \frac{t_T}{t_F} \tag{3-6}$$

where

$$t_F = \frac{l_F}{u_L} \tag{3-7}$$

$l_F$ is the flame thickness and $u_L$ is the laminar burning velocity. Define the Karlovitz number as

$$K = \left(\frac{l_F}{\eta}\right)^2 = \frac{t_F}{t_\eta} \tag{3-8}$$

Based on the integral scales a turbulent Reynolds number may be defined as

$$R_L = \frac{u'l}{\nu} \tag{3-9}$$

The turbulence Reynolds number has a more direct coupling to the structure of turbulence than the ordinary Reynolds number. It is apparent that $R_L < Re$.

## 3.2 Laminar Flamelets

Requirements for the applicability of thin laminar flamelet models can be identified by plotting, for example, the logarithm of the ratio of the fluctuating velocity to the laminar burning velocity versus the logarithm of the ratio of the integral length scale to the flame thickness. Different burning regimes may be identified in the diagram in terms of Damkohler, Karlovitz and turbulence Reynolds dimensionless numbers, figure 3.1 (Libby et al, 1994). The laminar flamelet regime is defined to lie below the line $K = 1$ (K=Ka) and above and to the right of the line $Re = 1$ to avoid low Reynolds number effects. The line $K = 1$ is called the Klimov-Williams line. The flamelet regime is where $K < 1$ so $l < \eta$ and the smallest scales of turbulence can not

enter the laminar flame structure. The Damkholer number is always $Da > 1$ (fast chemistry) and this means that the time scales associated with turbulence are always greater than those associated with combustion.

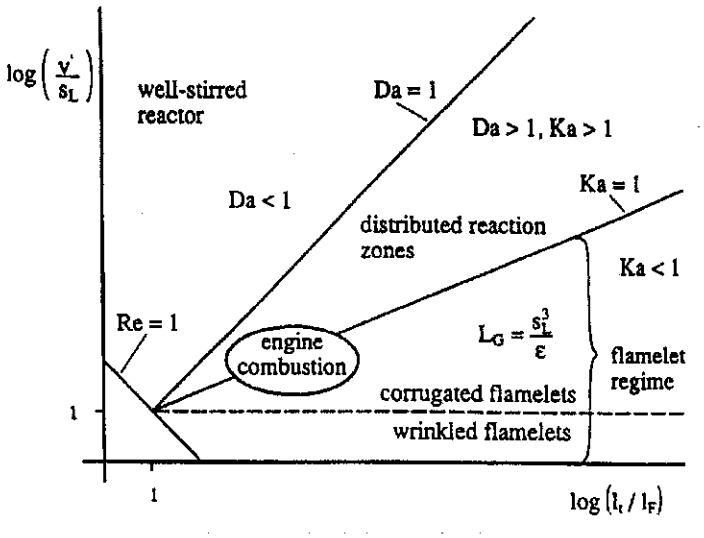


**Figure 3.1. Burning regimes in premixed turbulent combustion. Here $S_L = u_L$.**

The structure of a turbulent premixed flame can be viewed by superposition of instantaneous reaction fronts at different times, figure 3.2 (Turns, 1996).

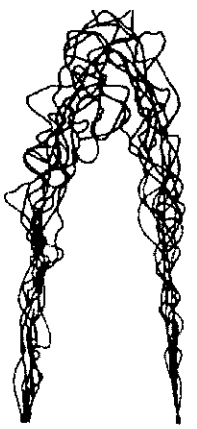

**Figure 3.2. Superposition of instantaneous reaction fronts at different times.**

The instantaneous view shows that the reaction fronts are relatively thin as in a laminar premixed flame. These thin reaction fronts are sometimes referred to as laminar flamelets. The laminar flamelet concept views a turbulent flame as an ensemble of thin locally one-dimensional structures within the turbulent flow field. In the flamelet approach, the chemical time scales are much smaller than the time scales associated with the turbulence. The eddies connected to the turbulence cannot change the local structure of the flame and this is the reason why a turbulent flame can be viewed as an ensemble of locally laminar flames, called flamelets.

# 4 Combustion Regimes of SI Engines

In premixed turbulent combustion, a flame propagates through a turbulent, molecularly mixed region of fuel and oxidizer. The flame is characterized by the relative values of various chemical and turbulence scales. Dimensional analysis reveals a range of premixed combustion modes progressing from wrinkled laminar flamelets, to well-stirred reactors. These modes correspond to different regimes of reaction and require different approaches for both understanding and modelling. Experimental as well as theoretical evidence suggests that many technologically important flows occur in the flamelet burning mode. Flamelet combustion corresponds to chemical reaction occurring at fast time scales and short length scales relative to turbulence. In this situation, the flame is confined to a relatively thin layer. In the flamelet regime, the local flame is very thin and the dominant effect of turbulence is to increase the flame surface area and to strain the local flame. The framework for modelling is therefore greatly simplified. It is then possible to describe the flame-flow interactions in terms of two quantities: the total flame front surface area, and the local flame structure (that is, the effects of turbulence and flame strain on the local laminar-like flame speed and the flame thickness).

Regimes of turbulent combustion can be viewed in many different diagrams. Several investigators have used ratios to develop diagrams that illustrate the different regimes of turbulent premixed combustion, an example of which is shown in figure 4.1(Abraham et al, 1985). From the perspective of the present work, of most interest in this figure is the estimate of the regime of SI engine operation. The different regimes indicated in the figure apply to premixed flames. Any one of the types of CFD approaches, which will be discussed on the next chapter may be expected to perform better in one of the regime, than in another. It is therefore of interest to try to identify where in the diagram the approach is used.

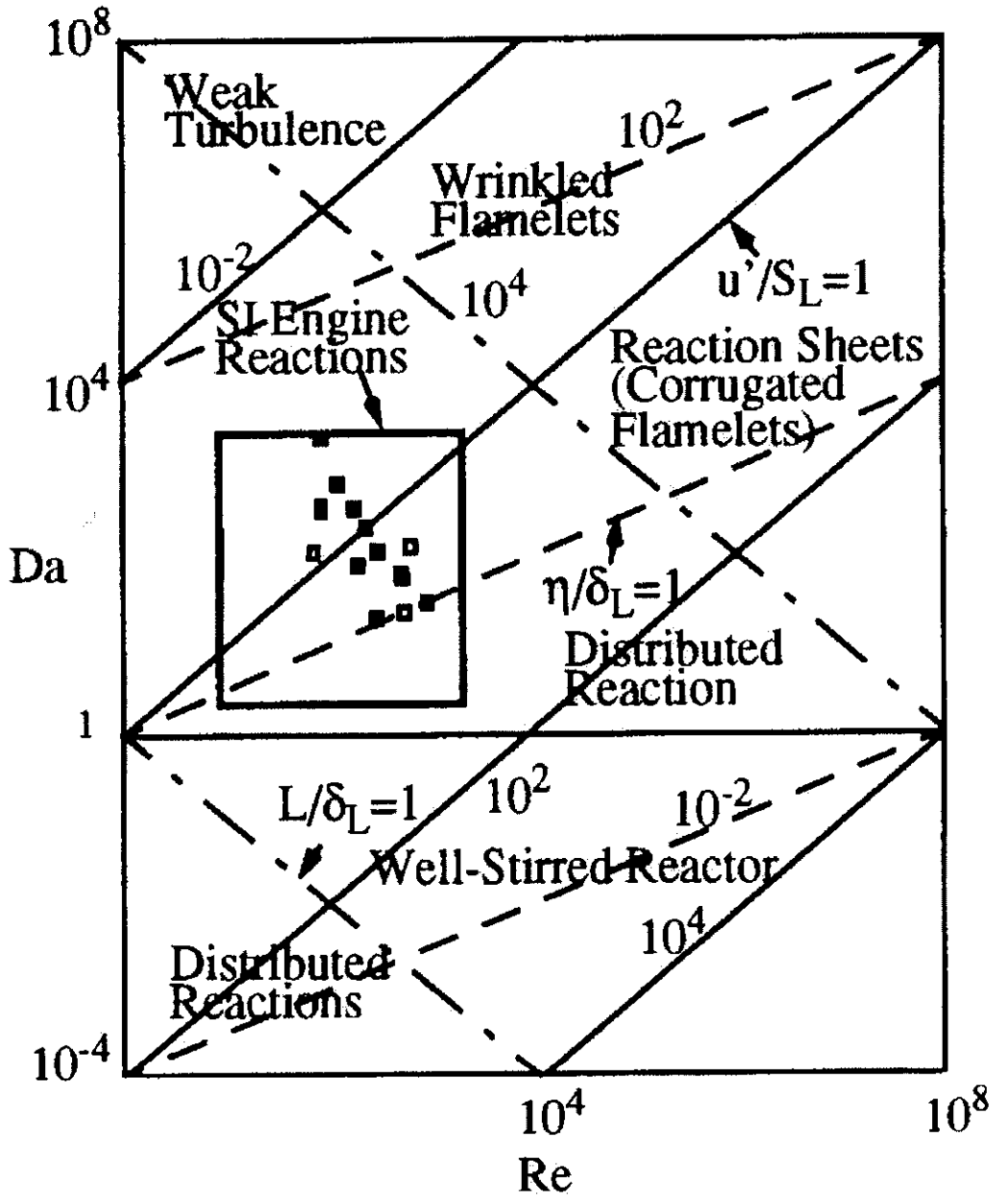


**Figure 4.1. Illustration of Regimes of Turbulent Combustion. The rectangle identifies the regime of engine operating conditions (Abraham et al, 1985)**

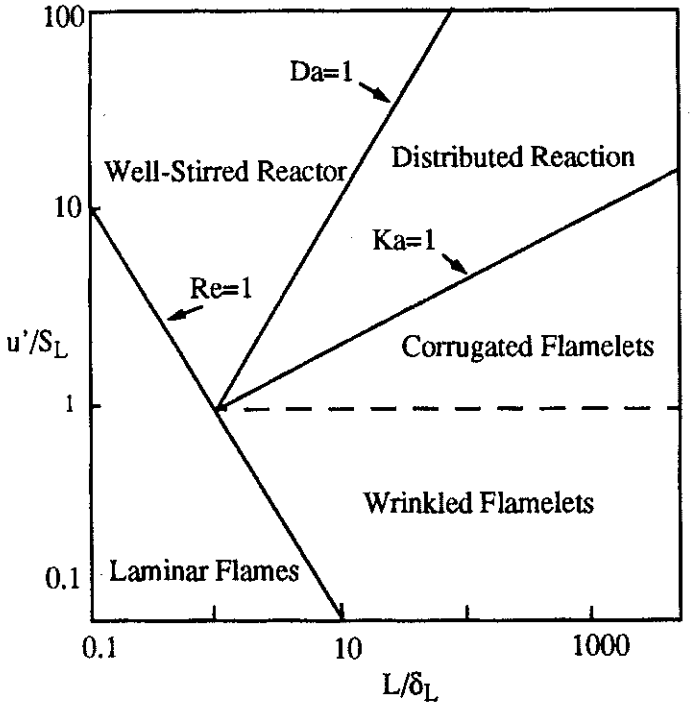


**Figure 4.2. Combustion regimes proposed by Borghi (1985) with terminology of Peters (1986)**

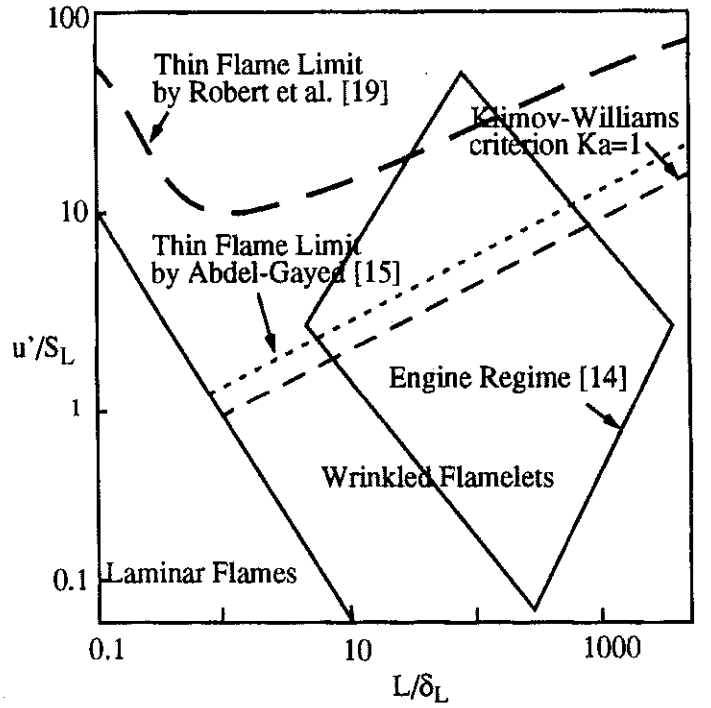


**Figure 4.3. A modified Borghi diagram illustrating the engine regime (from Abraham et al.) and shifting thoughts regarding the extent of the flamelet regime, including a revised thin flame limit by Abdel-Gayed et al, 1989. The diamond represent the rectangle regime corresponding to the engine combustion regime**

Another example is the modified Borghi diagram that is shown in figures 4.2 and 4.3. Figure 4.2 illustrates the regime of turbulent premixed combustion proposed by Borghi (1985) using Peter's (1986) terminology. Figure 4.3 is another modified Borghi diagram in which we have transposed the engine regime from Figure 4.1 and also illustrated that thoughts regarding the upper extent of the flamelet regime have changed significantly over the past few years. While there is uncertainty regarding the extent of the engine regime, especially considering that this regime was based upon Reynolds number and Damkohler number arguments rather than the $u'/S_L$ and $L/\delta_L$ parameters that define Figure 4.3, it appears that SI engines operate primarily within the flamelet regime.

# 5 Combustion Model

In CFD, all equations are averaged which leads to additional unknown terms, the Reynolds stress and the turbulent scalar flux, the second moments. The second moments appear as unknowns in the first moment equations (the averaged equations). The new unknowns have to be modelled and there are four main categories of turbulence models, viz., Algebraic (zero-equation) models, One-Equation models, Two-Equation models and Second Moment Closure models. The Standard k-ε Model is an example of a Two-Equation model and it is well known that this model have serious limitations. Closures at the second moment level represent a reasonably detailed description of turbulence at an acceptable level of complexity. The Reynolds Stress Model is an example of closure at the second moment level.

The equations are then solved numerically. To solve the equations numerically, the equations have to be discretised. The discretisation is achieved by approximating the governing equations with algebraic expressions. Interpolation is then used to get values at the surface of the control volume and there are several ways to do this.

## 5.1 Turbulence Modelling

There are a few ways possible for numerical prediction of a turbulent flow. These ways still range from a solution of the steady Reynolds- Averaged Navier-Stokes (RANS) equations to a Direct Numerical Simulation (DNS), with Large-Eddy Simulation (LES) in between.

Currently a very active area of research is the extension of DNS to LES in which large-scale time-dependent eddies are resolved while smaller sub-grid scale effects are modelled, where the necessary sub-grid modeling is by far the principal source of difficulty. However, uncertainties remain on the appropriate mathematical description of a turbulent flame interacting with sub-grid scales, and a critical

parameter requiring closure is the mean rate of reaction. Both DNS and LES are useful tools, but for engineering problems, Reynolds averaged numerical methods (RANS) have also shown to be feasible, hence will be used and discussed in detail, later in this chapter. For easier understanding the levels of different approaches to turbulent modelling, Figure 5.1 gives an overview on some of the approaches mentioned earlier.

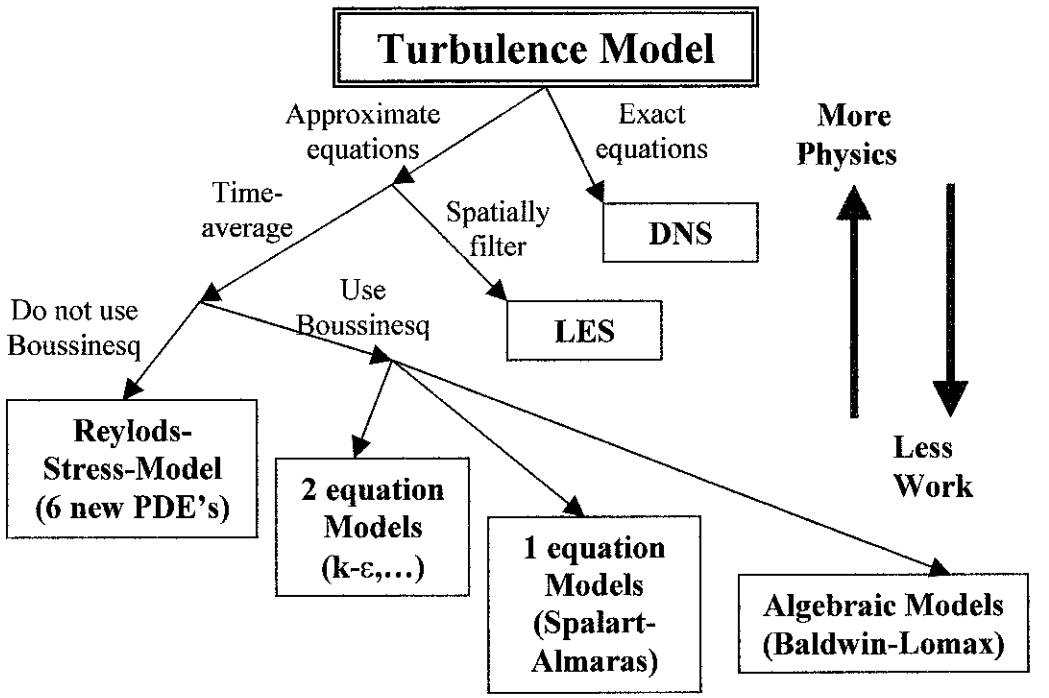


**Figure 5.1. Classification of Turbulence Models**

Recent years have added other strategies, URANS (Unsteady RANS) and DES (Detached Eddy-Simulation) for example. In DNS all the length and time scales of turbulence are resolved. The advantage of DNS is that no turbulence model is needed but the disadvantage is that it requires a lot of computational power and can only handle simple geometries with low Reynolds numbers. In LES, the governing equations are averaged using a space average. The space average also introduces unknown terms that have to be modelled. Very fine grids are required to resolve all length scales. URANS calculations are based on RANS models but are unsteady, even with steady boundary conditions. DES is a mixture of RANS and LES. In (Spalart, 2000), a summary of the strategies is made, see table 5.

**Table 5. Summary of Strategies**

| Name | Unsteady | Re-dependence | Empiricism | Grid | Ready |
|---|---|---|---|---|---|
| RANS | No | Weak | Strong | $10^7$ | 1990 |
| URANS | Yes | Weak | Strong | $10^7$ | 1995 |
| DES | Yes | Weak | Strong | $10^8$ | 2000 |
| LES | Yes | Weak | Weak | $10^{11.5}$ | 2045 |
| DNS | Yes | Strong | None | $10^{16}$ | 2080 |

Column 4 refers to, if the strategy depends on empirical relations, column 5 represents the number of grid points for a certain case and the readiness estimates are based on that computer power increases by a factor 5 every five years.

## 5.2 Reynolds-Averaged Navier-Stokes equations (RANS)

Reynolds averaged Navier-Stokes equations (RANS) equations were derived in 1895 by Osborne Reynolds who started from the assumption that each flow variable could be decomposed into a non-fluctuating, or mean, component plus a randomly fluctuating, or turbulent, component. Reynolds rewrote the Navier-Stokes equations by substituting the expanded form of the variables and averaging the equations over time in a procedure, which later became known as Reynolds averaging. In doing this, it throws away all of the details concerning the state of the flow contained in the instantaneous fluctuations.

For most engineering purposes it is unnecessary to resolve the details of the turbulent fluctuations. Only the effects of the turbulence on the mean flow are usually seek for. As the result of the time-averaging operation, obtained are additional unknowns called the Reynolds stresses. The equations that are used to model these unknown terms are called turbulence models. Once a turbulence model is decided, a closed set of equations is obtained, which than can be applied to the flow. Common classical RANS solvers use models such as the mixing length model, or the k-$\varepsilon$ model. They are based on the presumption that there exists an analogy between the action of viscous stresses and Reynolds stresses on the mean flow.

The disadvantage with the Reynolds stress model is that it increases the number of averaged equations, which leads to an increased number of terms to model. The price to be paid is in complexity and computational difficulty for the gains.

Meanwhile, the advantage of RANS is its applicability to any configuration and operating conditions: a standard RANS mesh can contain $10^5$ points and the domain of calculation may be as large as needed (Poinsot and Veynante, 2001). Hence, combustion chamber geometries may be analysed with such methods.

## 5.3 Project Aim

The aim of this Master Thesis is evaluation and validation of the newly developed moment based unstructured 2D Rans code called Turbulence Reactance Flow 2 Dimensional (TRF2D), which contains full closures at the second moment level for velocity and scalar fields. The newly developed code will be compared with an experimental data with test cases that contains swirl, recirculation and combustion with the use of the mounted obstacles to allow the build-up of turbulence which will then provide a challenging case studies. A further review on the investigation of flame/solid interactions in turbulent premixed combustion for model validation is well presented by Ibrahim et al, 2001.

Work is focused at improving the understanding of the processes involved, and providing a model that can be used as a design tool. In particular, to improve the computer modelling of combusting flows. A model for turbulent combustion must represent the turbulence, the combustion, and their interaction.

In general, the objectives of the development for more accurate combustion models are:

- To have an initial understanding of Combustion Phenomena.
- To have an understanding on the development of Computational Fluid Dynamics (CFD) code that will aid on the combustion observation.

- To simulate combustion process and then develop/improve its predictive capability.
- And most importantly, to develop a combustion code that is capable to take some of the cost when designing an SI engine, which consist of expensive experiments.

# 6 Governing Equations and Modelling Technique Used

The computer simulations of the experimental work were carried out using an in-house CFD code develop at Loughborough University called Turbulence Reactance Flow 2-Dimension (TRF2D). As in all CFD models, TRF2D solves for the fundamental governing equations of fluid motion, which contain all the physics for that problem. These equations can be solved for laminar flow and in principle can also be applied to turbulent flows. TRF2D solves for the following Navier-Stokes equations conservation of mass (continuity equation), conservation of momentum for each independent direction and conservation of total energy.

In addition to this, where the problem contains turbulent combustion transport equations are needed to model the turbulence effects. The equations solved by TRF2D to model the turbulence are transport of turbulent kinetic energy and transport of turbulent dissipation rate.

The numerical methods used in TRF2D can be classified into four categories: chemical kinetics, averaging techniques, turbulence modelling and reaction rate modelling, which will be discussed in greater detail in this chapter.

## 6.1 Chemical Kinetics

The thermodynamic laws allow the determination of the equilibrium state of a chemical reaction system. If one assumes that chemical reactions are fast compared to other processes like molecular transport, and flow, thermodynamics can be used to describe the system locally. In most cases, chemical reaction occurs on time scales comparable with that of the flow and of the molecular transport processes. Therefore, information is needed about the rate of chemical reaction, i.e., the chemical kinetics. Thus the basic laws of chemical kinetics shall be discussed in the following.

The so-called rate law shall be discussed for a chemical reaction, which is in general case can be described by the equation:

$$A + B + C + \ldots\ldots \xrightarrow{k} D + E + F + \ldots\ldots \tag{6-1}$$

where *A, B, C*.... denote the different species involved in the reaction. Hence, the reaction rate can be expressed according to

$$\frac{d[A]}{dt} = -k[A]^a[B]^b[C]^c.... \tag{6-2}$$

where *a, b, c* .... are the reaction orders with respect to the species *A, B, C* .... and *k* is the rate coefficient of the reaction.

For a reverse reaction, the rate law for the production of *A*

$$\frac{d[A]}{dt} = k^r[D]^d[E]^e[F]^f.... \tag{6-3}$$

Where the reverse reaction is characterized by the superscript *r*. At chemical equilibrium, forward and backward reactions have the same rate on microscopic level. Therefore, at chemical equilibrium one has

$$k^{(f)}[A]^a + [B]^b + [C]^c .... = + k^{(r)}[D]^d + [E]^e + [F]^f .... \tag{6-4}$$

Where the forward reaction is characterized by the superscript *f*. In general the equation of an elementary reaction is given by (Warantz et al. 1996):

$$\sum_{s=1}^{S} v_{rs}^{(e)} A_s \xrightarrow{k_r} \sum_{s=1}^{S} v_{rs}^{(p)} A_s \tag{6-5}$$

Here $v_{rs}^{(e)}$ and $v_{rs}^{(p)}$ denote stoichiometric coefficients of reactance (sometime called educts) or reactance. Then the rate law for the formation of species *i* in reaction *r* is given by the expression

$$\left(\frac{\partial c_i}{\partial t}\right)_{chem,r} = k_r\left(v_{ri}^{(p)} - v_{ri}^{(e)}\right)\prod_{s=1}^{S} c_s^{\nu rs^{(e)}} \qquad (6\text{-}6)$$

where $c_s$ denotes the concentration of S different species s. Therefore, the rate of formation of a species $i$ is given by summation over the rate equations (6-6) of all elementary reactions,

$$\left(\frac{\partial c_i}{\partial t}\right)_{chem} = \sum_{r=1}^{R} k_r\left(v_{ri}^{(p)} - v_{ri}^{(e)}\right)\prod_{s=1}^{S} c_s^{\nu rs^{(e)}} \quad \text{with} \quad i = 1,..,S. \qquad (6\text{-}7)$$

For simple combustion such as hydrogen and oxygen requires 40 elementary reactions, meanwhile for simple hydrocarbon fuels, such as methane $CH_4$, inhibit much larger number of elementary equations. In some cases several thousands of elementary reactions are present, for example, when Diesel is auto-ignited. These elementary equations can be used to obtain rate laws of each species and if parameters for computing the rate coefficients are available then the reaction rate of species $i$ can be computed within reasonable time frame. However, in instances when the number of species involved in a reaction is so large there is a risk of demanding prohibitive amount of computational time.

## 6.2 Averaging Technique

The work here is done according to the favre average concept. Not only Navier Stokes equations will be averaged with this concept but turbulence and combustion models also need to be averaged in order to close the equations. Using time-averaging, a mean can be obtained which is equal to the ensemble avereage, for example as shown by Warnatz et al, 1996. If the time behaviour of a variable is observed, e.g., the density $\rho$, it can be seen that the value fluctuates about an average. In a statically stationary process the time-average is obtained by integration over a long (ideally infinitely long) time interval,

$$\bar{\rho}\left(\vec{r}\right)=\lim_{\Delta t\to\infty}\frac{1}{\Delta t}\int_{0}^{\Delta t}\rho\left(\vec{r},t\right)dt \tag{6-8}$$

If the average itself is changing in time, local time averages can be calculated in non-stationary systems, if the temporal fluctuations are fast compared to the time-behaviour of the mean value. In this case the result for the time average at $t'$ ($t_1<t'<t_2$) is

$$\bar{\rho}\left(\vec{r},t'\right)=\frac{1}{t_2-t_1}\int_{t_1}^{t_2}\rho\left(\vec{r},t\right)dt \tag{6-9}$$

Now, the value of a function $q$ shall be split into its mean and the fluctuation (indicated by the apostrophe),

$$q\left(\vec{r},t\right)=\bar{q}\left(\vec{r},t\right)+q'\left(\vec{r},t\right) \tag{6-10}$$

If $q$ is averaged, the important result is that the mean of the fluctuation is zero,

$$\overline{q'}=0 \tag{6-11}$$

Large density variations are typical for combustion process. Thus it is useful to introduce another average, namely the Favre-average (also called density weighted average), which is, for an arbitrary property $q$, given by

$$\tilde{q}=\frac{\overline{\rho q}}{\bar{\rho}} \qquad \text{or} \qquad \bar{\rho}\tilde{q}=\overline{\rho q} \tag{6-12}$$

As in (4.12), any property $q$ again can be split into its mean value and the fluctuation,

$$q\left(\vec{r},t\right)=\tilde{q}\left(\vec{r},t\right)+q''\left(\vec{r},t\right) \tag{6-13}$$

and the results for the average of the Favre fluctuation (which is characterised by two apostrophes) is

$$\overline{\rho q''} = 0 \tag{6-14}$$

Introduction of (4.12) into (4.14), leads to a relation which formally allows the calculation of the Favre average from the average of a variable $q$,

$$\tilde{q} = \bar{q} + \frac{\overline{\rho' q'}}{\bar{\rho}} \tag{6-15}$$

In the following, additional relation for the averages are derived and the mean of the square of a variable q is easily calculated from (4.12)

$$\overline{q^2} = \bar{q}^2 + \overline{q'^2} \tag{6-16}$$

The density weighted mean of the correlation between the two variables u and v can be calculated according to

$$\begin{aligned} \overline{\rho u v} &= \overline{(\bar{\rho} + \rho')(\bar{u} + u')(\bar{v} + v')} \\ &= \overline{\rho u v} + \bar{\rho}\overline{u'v'} + \bar{u}\overline{\rho' v'} + \bar{v}\overline{\rho' u'} + \overline{\rho' u' v'} \end{aligned} \tag{6-17}$$

Splitting into Favre average and Favre fluctuation leads to

$$\overline{\rho u v} = \bar{\rho}\tilde{u}\tilde{v} + \overline{\rho u'' v''} \tag{6-18}$$

## 6.2.1 Averaged Equations

The Favre averaged governing conservation equations for mass, momentum, internal energy, and reaction progress variable can be written as:

where $\bar{\rho}$ is the mean density, $\phi = 1, \tilde{u}_j, \tilde{e}, \tilde{c}$, and $\tilde{}$ denotes Favre average. Complete closure of the above system of transport equations requires the closure of the turbulent transport term, $\overline{\rho u_i'' \phi''}$ (turbulence model) and the mean rate of chemical reaction, $\overline{W}$ (combustion model).

## 6.3 Turbulence Models

There are many models determining the turbulent exchange coefficient. The most two popular models are k-ε models and non-linear k-ε models.

### 6.3.1. The Standard k-ε Model

The turbulence transport or sometimes known as the turbulent diffusion term $\overline{\rho u'' \varphi''}$, can be closed using a standard k-ε model in which transport equations of the turbulence kinetic energy, k and it's dissipation rate, ε are solved. The scalar transport or diffusion term is then modelled using a simple gradient transport model.

$$\frac{\partial \overline{\rho u_i'' \phi''}}{\partial x_i} = \frac{\mu_t}{\sigma_\phi} \frac{\partial^2 \tilde{\phi}}{\partial x_i^2} \tag{6-25}$$

where $\mu_t$ is the turbulent viscosity calculated from:

$$\mu_t = \bar{\rho} C_\mu \frac{\tilde{k}^2}{\tilde{\varepsilon}} \tag{6-26}$$

Where $C_\mu$ is a dimensionless constant of value 0.09. In the standard k-ε model, Boussinesq eddy-viscosity approximation assumes to be valid and therefore, the Reynolds stress tensor given by

$$\overline{\rho u_i'' u_j''} = \mu_t \left( \frac{\partial \tilde{u}_i}{\partial x_j} + \frac{\partial \tilde{u}_j}{\partial x_i} \right) - \frac{2}{3} \bar{\rho} \tilde{k} \frac{\partial \tilde{u}_i}{\partial x_i} \tag{6-27}$$

Transport equations are used to obtain the turbulence kinetic energy, $\widetilde{k}$, and its rate of dissipation, $\widetilde{\varepsilon}$ (as shown by Patel, 2001)

$$\frac{\partial \overline{\rho}\widetilde{k}}{\partial t}+\frac{\partial \overline{\rho}\widetilde{u}_i\widetilde{k}}{\partial x_i}=\frac{\mu_t}{\sigma_{\widetilde{k}}}\frac{\partial^2\widetilde{k}}{\partial x_i^{\,2}}+S_k \tag{6-28}$$

$$\frac{\partial \overline{\rho}\widetilde{\varepsilon}}{\partial t}+\frac{\partial \overline{\rho}\widetilde{u}_i\widetilde{\varepsilon}}{\partial x_i}=\frac{\mu_t}{\sigma_{\widetilde{\varepsilon}}}\frac{\partial^2\widetilde{\varepsilon}}{\partial x_i^{\,2}}+S_\varepsilon \tag{6-29}$$

Where $S_k$ and $S_\varepsilon$ are the source/sink terms of the turbulence kinetic energy and its dissipation rate, respectively.

$S_k$ is modelled as:

$$S_k = P-\overline{\rho}\widetilde{\varepsilon} \tag{6-30}$$

where P is the production of $\widetilde{k}$ due to the mean velocity gradients:

$$P=\mu_t\left(\frac{\partial\widetilde{u}_i}{\partial x_j}+\frac{\partial\widetilde{u}_j}{\partial x_i}\right)\frac{\partial\widetilde{u}_i}{\partial x_i} \tag{6-31}$$

and $S_\varepsilon$ is modelled as:

$$\frac{\widetilde{\varepsilon}}{\widetilde{k}}\left(C_{\varepsilon 1}P-C_{\varepsilon 2}\overline{\rho}\widetilde{\varepsilon}\right)+C_{\varepsilon 3}\overline{\rho}\widetilde{\varepsilon}\frac{\partial\widetilde{u}_i}{\partial x_i} \tag{6-32}$$

In summary, the standard k-ε model is an example of a Two-Equation model and this means that closure is obtained through two extra partial differential equations, one for the turbulence kinetic energy, $k$, and one for the turbulence dissipation rate, ε. $k$ and ε relation are defined as

$$\varepsilon = \frac{energy}{time} = \frac{k}{l/k^{1/2}} = \frac{k^{3/2}}{l} \tag{6-33}$$

Hence, arranging the equation gives the relationship for the scale of turbulence, $l$

$$l = \frac{k^{3/2}}{\varepsilon} \tag{6-34}$$

The turbulent kinetic energy, k, can also be defined by the following equation:

$$k = \frac{1}{2}\left(u'^2 + v'^2 + w'^2\right) \tag{6-35}$$

Where u' is the turbulent velocity in the x direction, v' in the y direction and w' in the z direction.

The flow is assumed to be isotropic, hence u' = v' = w'

$$k = \frac{3}{2}\left(u'^2\right) \tag{6-36}$$

Then u' can be obtained:

$$u' = \sqrt{\frac{2k}{3}} \tag{6-37}$$

Since $l$ and $u'$ can be obtained, the turbulent Reynolds number $R_L$ (3-9) can now be calculated since the kinematic viscosity of the fluid, $v$, is known. The Damkohler number, $Da$ (3-6), can also be calculated since now the turbulent time, $t_T$ can be found and the flame time or the chemical reaction rate, $t_F$ is approximated to a constant value. Hence the regimes of combustion can now be identified.

### 6.3.2 Non-Linear k-ε Models

It is widely accepted that the linear eddy-viscosity type of turbulence models cannot, without modifications, account for the streamline curvature effect. Therefore, the natural route is to apply Second-Moment Closures in predicting the recirculating flows. The non-linear eddy viscosity models used is the Craft et al.'s (1993) formulation which returns the slowest rate of recovery and is consistent with the isothermal flow simulation (Kuo et al., 2000).Reynold stress here is modelled using the following cubic formulation:

$$\begin{aligned} -\rho\overline{u_i u_j} &= -\frac{2}{3}\delta_{ij}\rho k + \mu_t S_{ij} + C_1\frac{k}{\varepsilon}\mu_t[S_{ik}S_{kj} - \frac{1}{3}\delta_{ij}S_{kl}S_{kl}] \\ &+ C_2\frac{k}{\varepsilon}\mu_t[\Omega_{ik}S_{kj} + \Omega_{jk}S_{ki}] + C_3\frac{k}{\varepsilon}\mu_t[\Omega_{ik}\Omega_{kj} - \frac{1}{3}\delta_{ij}\Omega_{kl}\Omega_{kl}] \\ &+ C_4\frac{k^2}{\varepsilon^2}C_\mu\mu_t(S_{ki}\Omega_{lj} + S_{kj}\Omega_{li} - \frac{2}{3}S_{km}\Omega_{lm}\delta_{ij})S_{kl} \\ &+ C_6\frac{k^2}{\varepsilon^2}C_\mu\mu_t S_{ij}S_{kl}S_{kl} + C_7\frac{k^2}{\varepsilon^2}C_\mu\mu_t S_{ij}\Omega_{kl}\Omega_{kl} \end{aligned} \tag{6-38}$$

where $C_1 = -0.1, C_2 = 0.1, C_3 = 0.26, C_4 = -1, C_6 = -0.1, C_7 = 0.1$

and $C\mu$ is computed from

$$C\mu = \frac{0.3}{1+0.35[\max(S,\Omega)]^{1.5}}[1-\exp[-0.36/\exp(-0.75\max(S,\Omega))]] \tag{6-39}$$

The strain and vorticity tensors, $S_{ij}$ and $\Omega_{ij}$, and the strain and vorticity magnitudes, $S$ and $\Omega$ are computed from the following equations.

$$S_{ij} = \frac{\partial U_i}{\partial x_j} + \frac{\partial U_j}{\partial x_i} \tag{6-40}$$

$$\Omega_{ij} = \frac{\partial U_i}{\partial x_j} - \frac{\partial U_j}{\partial x_i} \tag{6-41}$$

$$S = \frac{k}{\varepsilon}\sqrt{S_{ij}S_{ij}/2} \tag{6-42}$$

$$\Omega = \frac{k}{\varepsilon}\sqrt{\Omega_{ij}\Omega_{ij}/2} \tag{6-43}$$

## 6.4 Reaction Rates

In order to solve the averaged conservation equations (6-19 to 6-22), one still has to specify the averaged chemical reaction rates $\overline{W}$, which will then lead to computation of the density and pressure.

Flamelet modelling provides a mean to introduce chemical and turbulence time scales by considering a thin laminar flame in a turbulent flow field. The key goals behind flamelet modelling are to incorporate effects of fast but finite reaction rates, the inherent quasi-laminar flame dynamics and the intimate coupling between chemical reactions and molecular transport that arises when rapid chemistry enforces very thin flame structures. Much of the flamelet modeling literature focuses on deriving effective turbulent burning velocity. The alternative modeling strategy has been pursued for the flamelet regime since the first introduction of the Bray-Moss-Libby model (BML). This approach is based on evaluating the flame surface area to volume ratio (flame surface density), $\Sigma$, which can be computed via an algebraic (Bray, 1990) or through a transport equation (Duclos et al., 1993). Then the local mean rate of reaction, $\overline{W}$, is calculated using:

$$\overline{W} = R\Sigma \tag{6-44}$$

where $R$ is the rate of reaction per unit area computed from

$$R = \rho_u u_L \tag{6-45}$$

where

$\Sigma$ is the flamelet surface density.

$\rho_u$ is the density of the unburnt mixture.

$u_L$ is the laminar burning velocity.

The flamelet surface surface density, $\Sigma$, can be calculated using either an algebraic formulation (BML model ) or a transport equation for $\Sigma$ (FSD model). However, only the BML model will be used and discussed here.

### 6.4.1 BML Model

The algebraic formulation for the flamelet surface surface density, $\Sigma$, is (Bray, 1990)

$$\Sigma = I_o g \frac{\tilde{c}(1-\tilde{c})(1+\bar{\tau})}{|\sigma_y| \hat{L}_y (1+\bar{\tau}\tilde{c})} \tag{6-46}$$

where

$\hat{L}_y$ is the flamelet wrinkling length scale.

$I_o$ is a factor correcting for mean effects of strain and curvature on the laminar flame.

$g$ is a constant whose value is fixed by the Probability Density Function (PDF) of the flamelet crossing process.

$|\sigma_y|$ is the cosine of the mean direction of crossing.

And $\bar{\tau}$ is the heat release parameter given by

$$\bar{\tau} = \frac{\bar{\rho}_u}{\bar{\rho}_b} + 1 \tag{6-47}$$

where $\rho_b$ is the density of the burnt mixture.

The closure for these controlling parameters has been adapted from the work of Patel and Ibrahim (1999). Thus the problem of modelling the mean rate of chemical reaction $\overline{\dot{w}} = R\Sigma$ has converted into modelling these controlling parameters.

The laminar burning velocity, $u_L$, is calculated using a simple algebraic expression due to Metghalchi and Keck (1980):

$$u_L = u_{L_o}\left(\frac{T_R}{T_o}\right)^{\alpha}\left(\frac{\overline{P}}{P_o}\right)^{\beta} \tag{6-48}$$

where

$u_{L_o}$ is the reference unstrained laminar burning velocity, taken here equal to 0.41 m/s for stoichiometric methane/air mixture.

$T_o$ and $P_o$ are reference temperature and pressure values (298.15 K, 1.01 bar), respectively.

$T_R$ is the reactant temperature and $\alpha$ and $\beta$ are constants with values 2.18 and –0.16, respectively (Turns 2000).

The $I_o$ factor is evaluated using (Bray, 1990)

$$I_o = \frac{0.117K^{0.784}}{1+\overline{\tau}} \tag{6-49}$$

where $K$ is the dimensionless Karlovitz stretch factor.

The Karlovitz stretch factor is evaluated from (Abdel-Gayed et al., 1987)

$$K = 0.157\left(\frac{u''}{u_L}\right)^2 R_L^{-0.5} \tag{6-50}$$

where

$u''$ is the RMS turbulent velocity.

$R_L$ is the turbulent Reynolds number based on the microscopic scale of turbulence.

$$\overline{\rho}\left(\vec{r}\right)=\lim_{\Delta t\to\infty}\frac{1}{\Delta t}\int_{0}^{\Delta t}\rho\left(\vec{r},t\right)dt \tag{6-8}$$

If the average itself is changing in time, local time averages can be calculated in non-stationary systems, if the temporal fluctuations are fast compared to the time-behaviour of the mean value. In this case the result for the time average at $t'$ ($t_1<t'<t_2$) is

$$\overline{\rho}\left(\vec{r},t'\right)=\frac{1}{t_2-t_1}\int_{t_1}^{t_2}\rho\left(\vec{r},t\right)dt \tag{6-9}$$

Now, the value of a function $q$ shall be split into its mean and the fluctuation (indicated by the apostrophe),

$$q\left(\vec{r},t\right)=\overline{q}\left(\vec{r},t\right)+q'\left(\vec{r},t\right) \tag{6-10}$$

If $q$ is averaged, the important result is that the mean of the fluctuation is zero,

$$\overline{q'}=0 \tag{6-11}$$

Large density variations are typical for combustion process. Thus it is useful to introduce another average, namely the Favre-average (also called density weighted average), which is, for an arbitrary property $q$, given by

$$\tilde{q}=\frac{\overline{\rho q}}{\overline{\rho}} \qquad \text{or} \qquad \overline{\rho}\,\tilde{q}=\overline{\rho q} \tag{6-12}$$

As in (4.12), any property $q$ again can be split into its mean value and the fluctuation,

$$q\left(\vec{r},t\right)=\tilde{q}\left(\vec{r},t\right)+q''\left(\vec{r},t\right) \tag{6-13}$$

# 7 Test Cases

The test case used in the project involved two stages. Firstly, to identify related experimental work that could be used for validation and secondly the set-up of the experimental modelling used to simulate the experimental results.

## 7.1 Related Experimental Work

The investigation of turbulent premix flame interaction with solid obstacles mounted inside semi-confined cylinderical vessel was carried out by Jarvis et al., 2001. The schematic diagram of the experimental rig is shown in figure 7.1. The hasting mass flow apparatus was used to fill the combustion chamber with a mixture of fuel and air of desired strength. The combustion chamber is made from clear polycarbonate to allow optical acces and has a dimension shown in figure 7.2, where the length of the tube is 500 mm and has a cross section of 150 × 150 $mm^2$. The chamber is closed at the bottom end and open at the top end. Three flat plate obstacles of rectangular cross-section 75 mm x 10 mm, providing a blockage ratio of 50% are mounted within the explosion unit centered and separated by 100 mm from the ignition end and from each other.

A single point spark-ignition was used placed at the center of the bottom end. During the experiment, the top end is covered with plastic film (diapragm) to trapped the premixed methane-air mixture used. Seeded particle are also added to the mixture to allow a copper vapour laser to trace flame propagation. Images of the flame propogation were recorded using a CCD camera operating at 40,000 frames per second. A high-speed Kistler Piezoresistive pressure tranducer was mounted at the closed end of the combustion chamber to record the pressure rise during the flame propogation. The pressure was recorded with 12 bit resolution at a rate of 20 kHz.

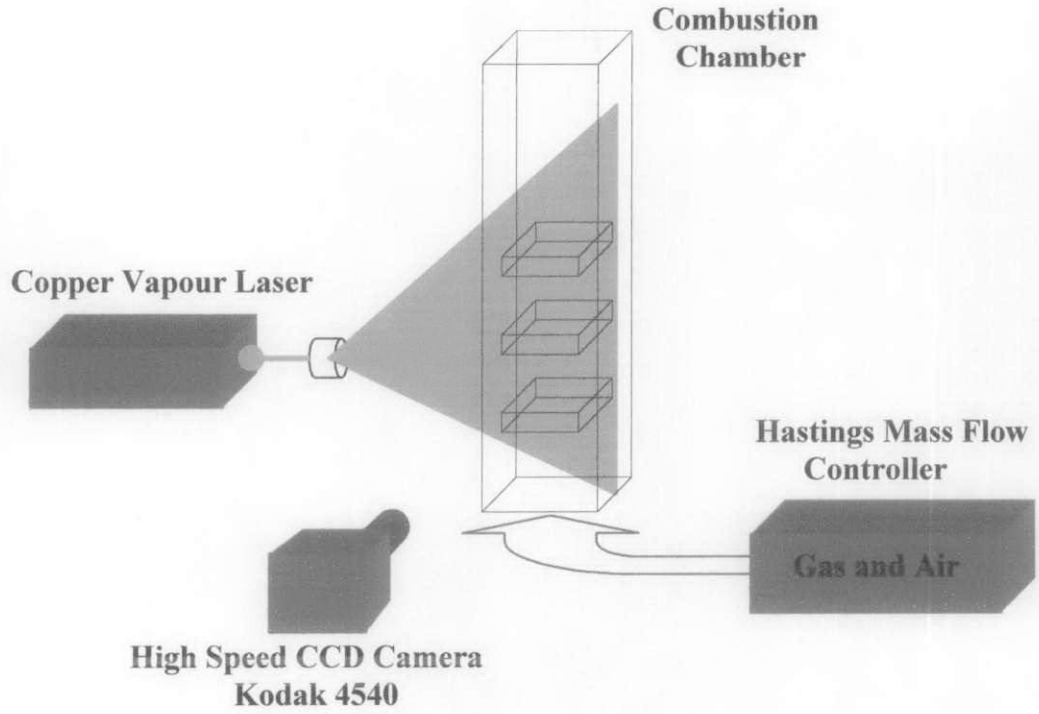


**Figure 7.1 Schematic of Experimental Test Rig (Jarvis et al., 2001).**

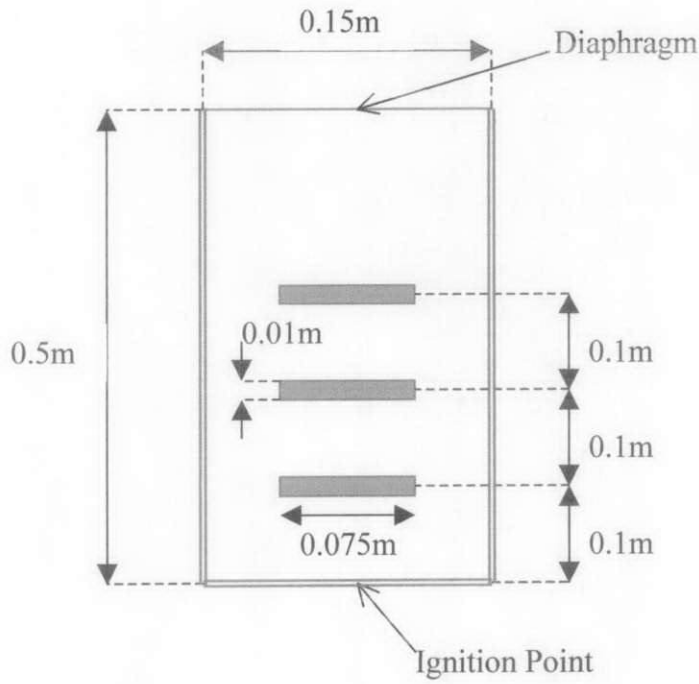


**Figure 7.2. Schematic diagram of the combustion chamber with three obstacles.**

The experimental results of the flame images at various time, flame front location versus time and the pressure versus time, at stoichimetric, were analysed so that the comparison between the experimental data and the predicted (calculated) data by TRF2D can be compared for the turbulent premixed combustion model validation.

## 7.2 Experimental Modelling

The computer simulation of the experimental work were carried out using TRF2D. Tecplot 8 is used as post-processor to generate the flame propagation images at different time steps. TRF2D solves the Favre averaged conservation equations for the mass (continuity), momentum, fuel mass fraction, mixture fraction, turbulence kinetic energy, rate of turbulence dissipation and flame surface density by linearising it using finite volume techniques. The linearised equations are then solved using Pressure Implicit Splitting Operation (PISO) solver from Issa, (1986). The computational Mesh applied to the geometry is set to be uniform and non-uniform, where the cells of the mesh are the finite volumes on which the conservative forms of the equation are applied. The grid used consist of 122 nodes in the i direction and 402 nodes in the j direction. The remaining boundaries outside the chamber were taken as outflow surfaces and the time step used was $6\times10^{-6}$ seconds. Modified BML model was applied near the wall boundaries to avoid unrealistic flame acceleration along the walls.

The same test geometry is used in TRF2D code (as in figure 7.2) so that comparisons of the results can be evaluated. The use of the mounted obstacles is to allow the build-up of turbulence and thereby generating different regimes of combustion. This also creates a complex interaction to be setup between the flame flow and obstacles, where flame flattening, jetting, reconnecting and venting are coexisting, hence provide a challenging problem for numerical model.

The validation of the numerical model is of importance if the model was going to be applied to other practical geometries like an IC engine geometry. From the

experiments carried out at Loughborough University by Jarvis et al (2001), the calculated result from TRF2D can be compared with experimental result.

# 8 Results and Discussion

By using a standard k-ε model, predicted results are simulated. In the standard k-ε model, Boussinesq eddy-viscosity approximation is assumed to be valid. Figure 8.1 demonstrates the comparison between high-speed images taken from laboratory experimental work and predicted flame structures calculated from reaction progress variable, c, of stoichiometric methane mixture (red-burned mixture and blue-unburned mixture) at different times after ignition using a standard k-ε model.

It can be seen that the calculated flame structure is very similar to that shown in the experimental studies. It was noted that at 24 ms the flame front for the experimental results is already flatten and the formed two flame 'tongues' around the side of the first obstacle is clear at 28 ms showing the interaction of the flame front with the turbulent wake behind the obstacle. Initially, although not shown, the flame is near laminar and has almost negligible turbulent structure. For the calculated flame structure, it also starts on the formation of the flame 'tongues' as flame front hit the first obstacle showing that the calculated results almost the same as experimental but only a little bit faster.

Just as the flame passes the first obstacle, it begins to interact with the recirculating flow behind the obstacle. For the experimental results, starting from the mixture directly behind the first obstacle, it remains unburned. Then as the flame propagates, reaching the second obstacle at around 32 ms, it is noted that the mixture behind the first obstacle is burned in recirculating manner due to the interaction of the flame with the highly turbulent flow directly behind the first obstacle. Whereas, the mixture of the fuel and air behind the first obstacle remain unburned for the calculated ones.

As the experimental flame progress further, the same phenomena of recirculation burning of fuel and air mixture takes place as it interacts with the third obstacle and at the same time the splitting flame front starting to reconnects. For the calculated flame front, it still shows no effect of this recirculation and flame reconnection as it passes an obstacle.

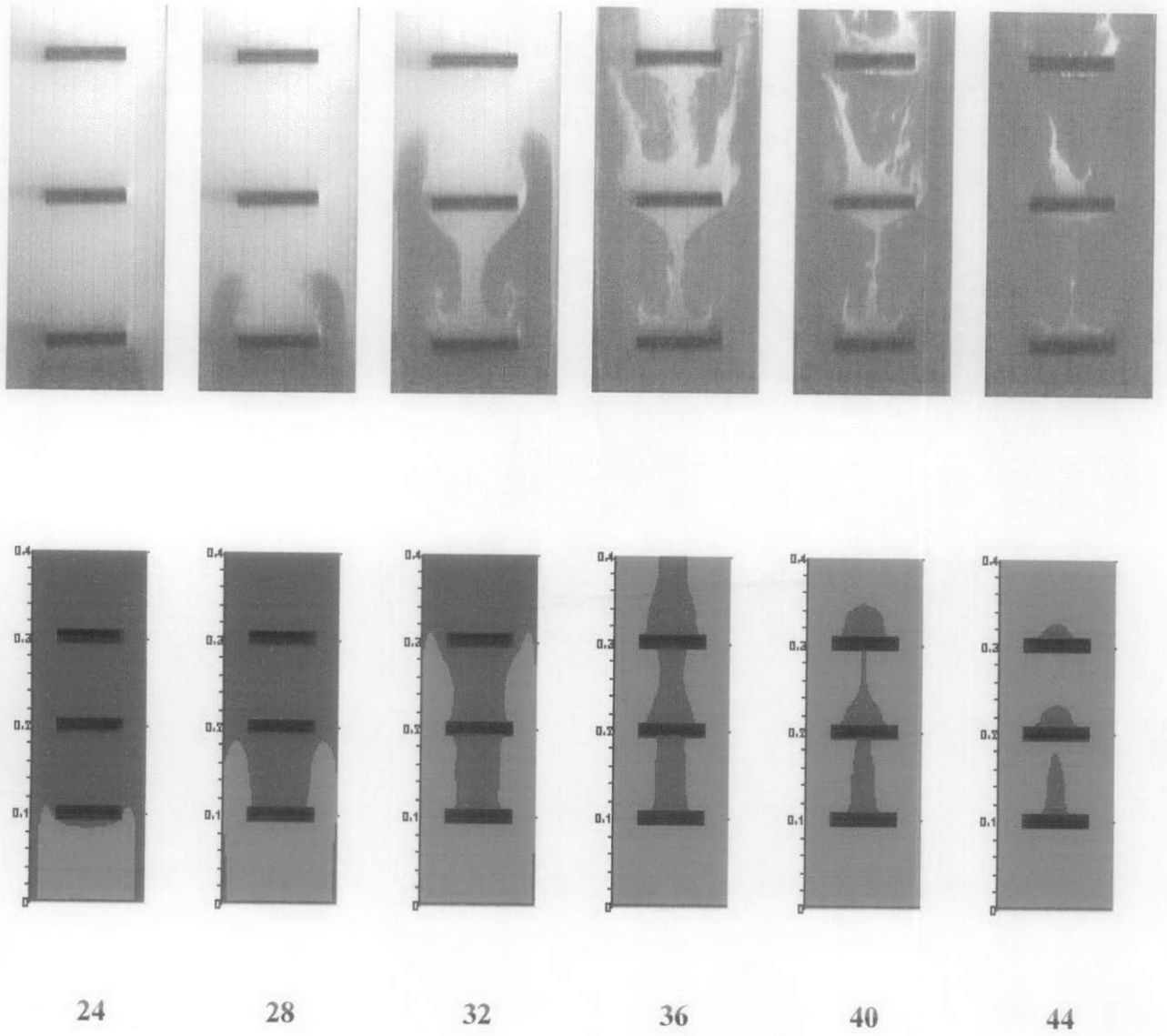


**Figure 8.1. Comparison of flame front structure of premixed methane at different times (ms) after ignition between high speed images (top) and calculated (bottom) using the standard k-ε model. Shown above are the images at 24 to 44 ms**

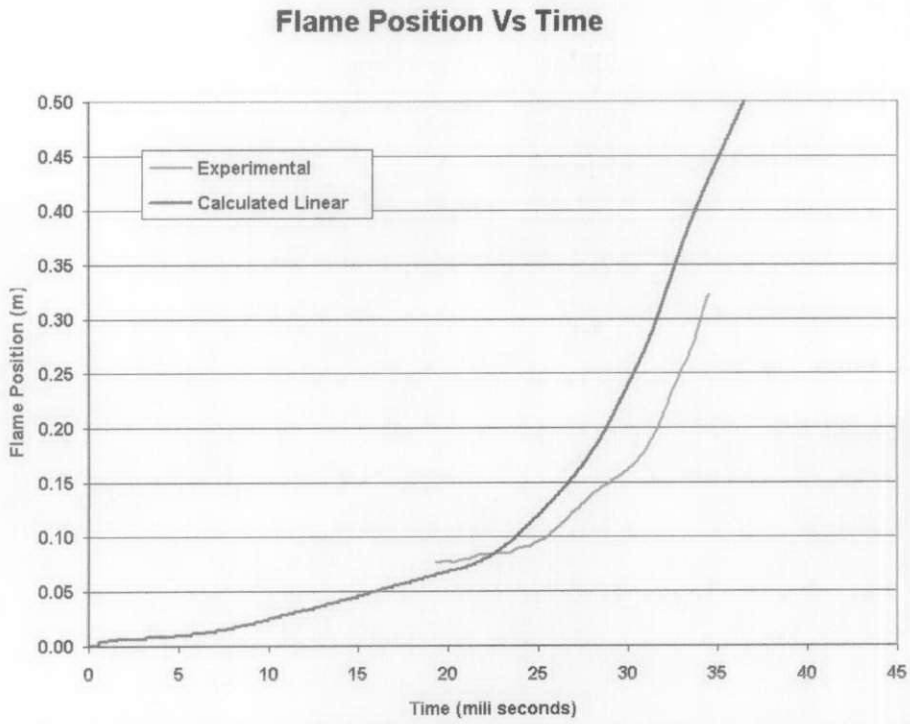


**Figure 8.2. Comparison of flame position of premixed methane after ignition between experimental and calculated using the standard k-ε model**

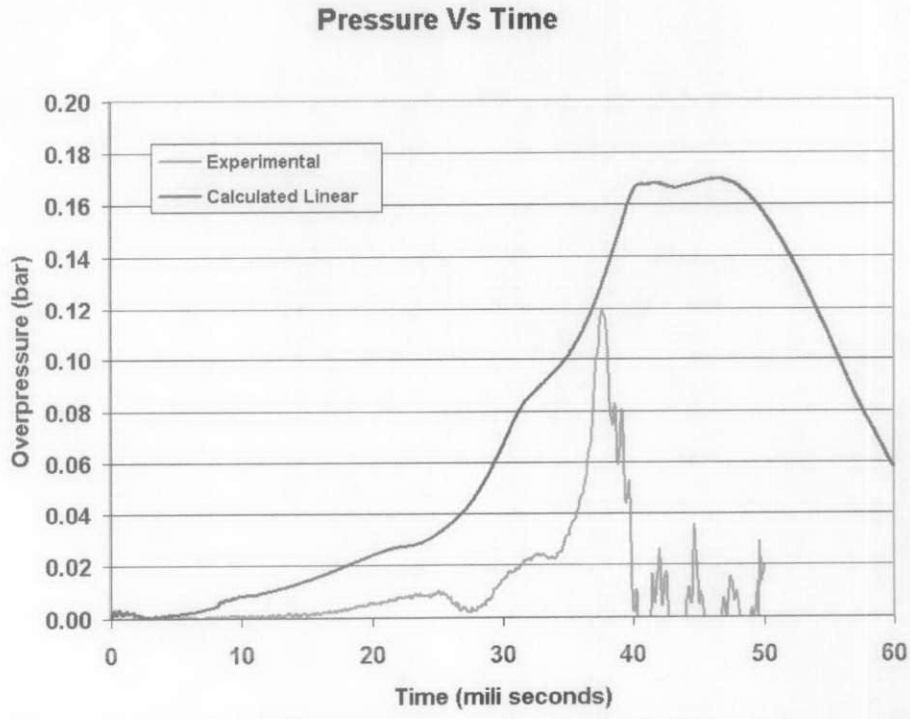


**Figure 8.3. Comparison of pressure time history of premixed methane after ignition between experimental and calculated using the standard k-ε model**

These suggest that the calculated flame have a lower turbulence presence in the chamber compared to experimental.

Another thing noted is the flame fronts of the experimental flame tongues are a bit distorted especially at the recirculation regions. Whereas, the calculated results show a smooth flame front. This is due to the effect of the averaging process used in the TRF2D code.

Also from the comparison of the flame position and pressure shown in figure 8.2 and 8.3. The calculated flame, most of the time, is ahead of the experimental result. This is confirmed from the comparison of the flame front structure shown earlier. Looking at the pressure time history figure 8.3, the experimental result shows that the pressure peaked and dipped every time the flame front passes the obstacles. This occurs at around 24, 32 and 36 ms respectively.

The peaks are due to the build up of the turbulence when the flame front interact with the obstacles and burning the trapped premixed mixture behind the obstacle. Meanwhile, the little dip takes place as the mixture is burned. The maximum peak formed as the flame propagate passes the last obstacle with a very high velocity and turbulent intensity, burning all the remaining methane mixture causing a blow-out, which then drastically drops as all the remaining mixture is already burned. It is clear that there is an over prediction on the pressure as the calculated pressure is all the time much higher than it should be, especially the maximum, where it peaked at a higher value (45 mbar over-prediction) and shows a later drop of pressure during the blow-out phase.

In an SI engine the pressure development is uniquely related to combustion process. The pressure in the combustion chamber is a measure of the rate of heat release. Therefore, it is important that the pressure time history predicted by the code follows the trend of the experimental results.

## 8.1 Investigation of Standard k-ε Model

In equation (6-26), the turbulent viscosity $\mu_t$ is calculated using dimensionless constant $C_\mu$ of value 0.09, which are suggested by many books to be the best value obtained from experimental results. From the predicted pressure result earlier, the over prediction might be due to the high combustion diffusion generated in the code. In this section, investigation of using different values of $C_\mu$ are simulated by reducing its value, which will then reduce the overall turbulence diffusion generated.

By reducing the value of $C_\mu$ (shown later in the plots as CMU) the predicted results generated by the code are investigated. Figure 8.4 and 8.5 shows the comparison of the flame front propagation generated with $C_\mu$ of a value 0.08, 0.07 and 0.06. The results show that, as the value of $C_\mu$ is reduced, the flame propagation gets slower and there is a better turbulence diffusion between obstacles. These phenomena could be seen at 36 ms where, as the value of $C_\mu$ is decreased, there is a slight increase of flame turning or recirculating between the first and second obstacles. The speed of the flames propagation are improved down to the value of $C_\mu = 0.07$ used. However, the modified standard k-ε model used still fail to generate the recirculation phenomena as the flame front passes the obstacles. Also, the model fails to produce realistic results when a value of 0.06 is used, as shown at 40 ms, a sudden total burned of mixture is simulated.

The improvements are again visible form the plots of the flame position and the pressure time history shown in figure 8.6 and 8.7, where the predicted results are getting closer to the experimental results. The failure of using a value of $C_\mu = 0.06$ is also visible as shown by the sudden increase in pressure.

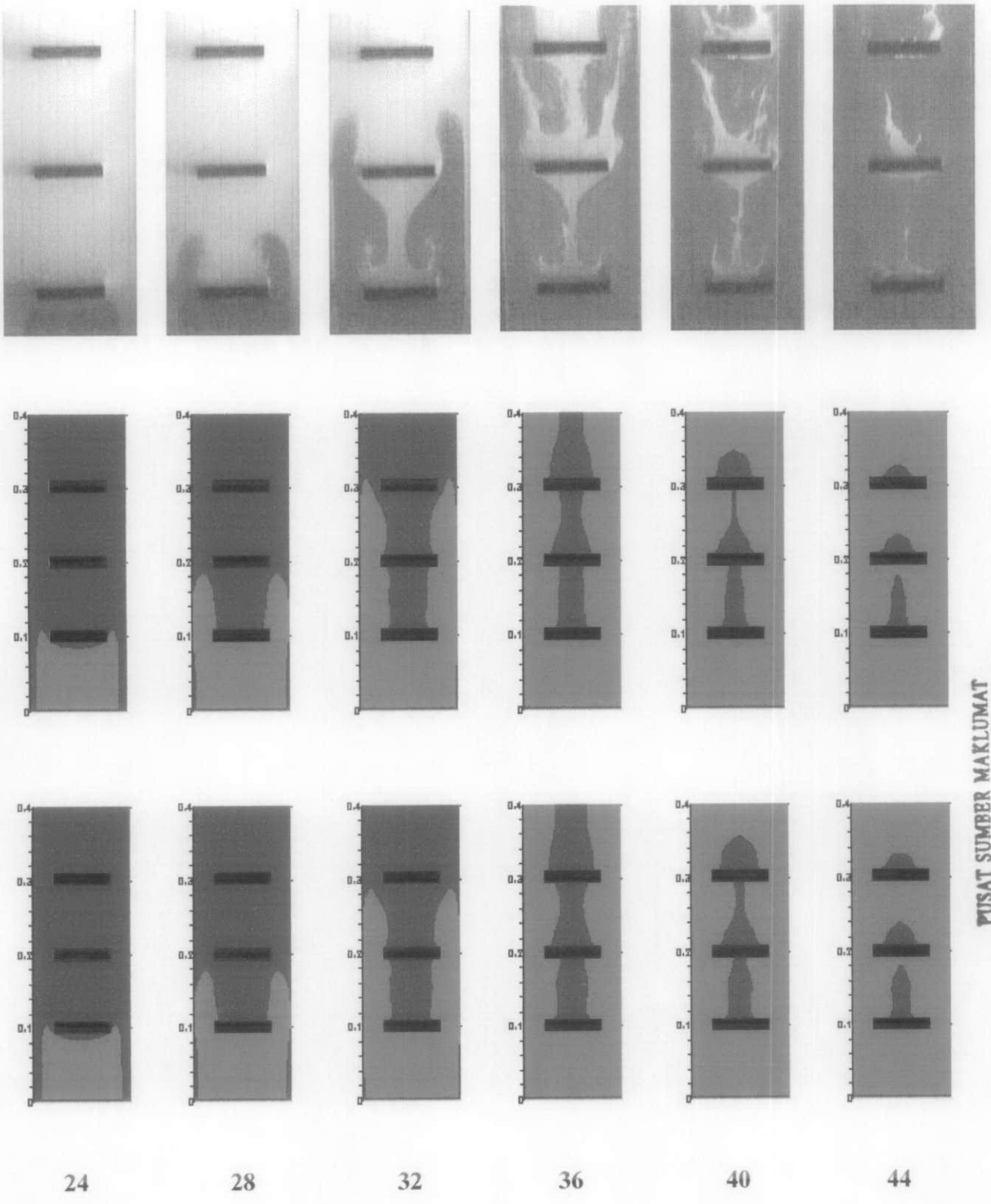




**Figure 8.4. Comparison of flame front structure of premixed methane at different times (ms) after ignition between high speed images (top), calculated (middle – using $C_\mu = 0.09$) and calculated (middle – using $C_\mu = 0.08$) using the standard k-ε model. Shown above are the images at 24 to 44 ms**

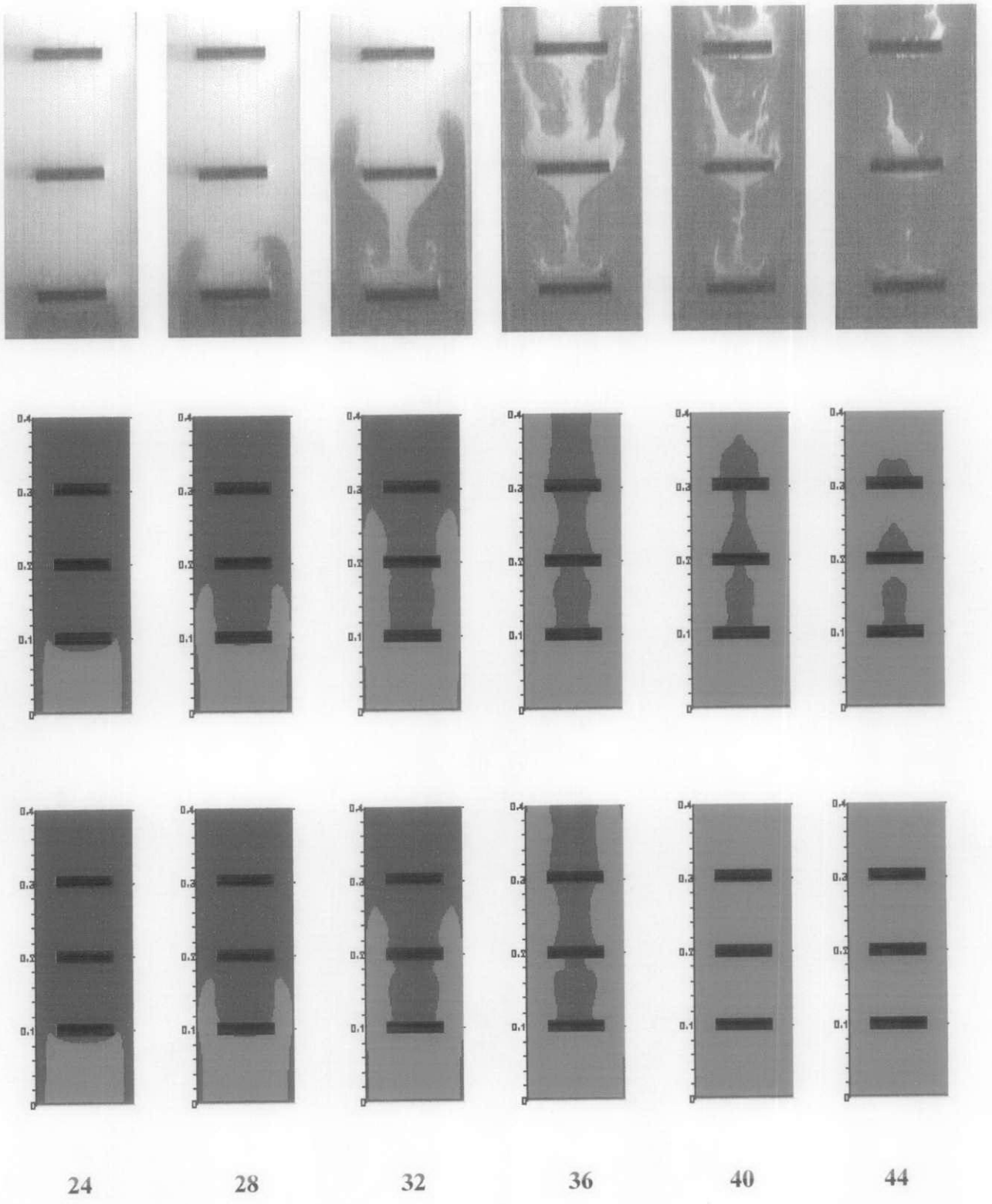


**Figure 8.5. Comparison of flame front structure of premixed methane at different times (ms) after ignition between high speed images (top), calculated (middle – using $C_\mu = 0.07$) and calculated (middle – using $C_\mu = 0.06$) using the standard k-ε model. Shown above are the images at 24 to 44 ms**

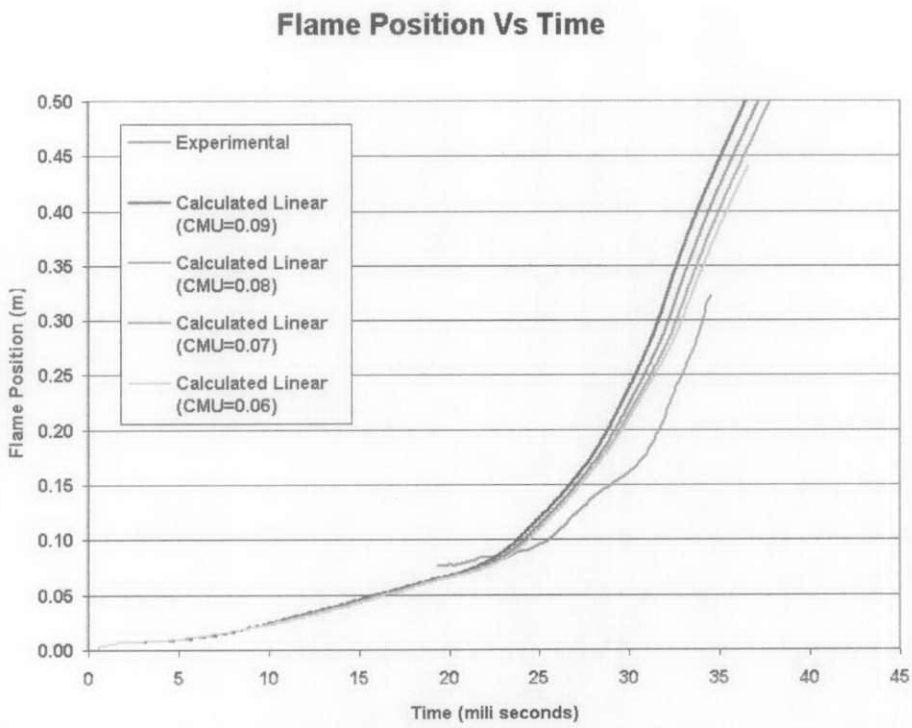


**Figure 8.6. Comparison of flame position of premixed methane after ignition between experimental and calculated using standard k-ε model (CMU=$C_\mu$)**

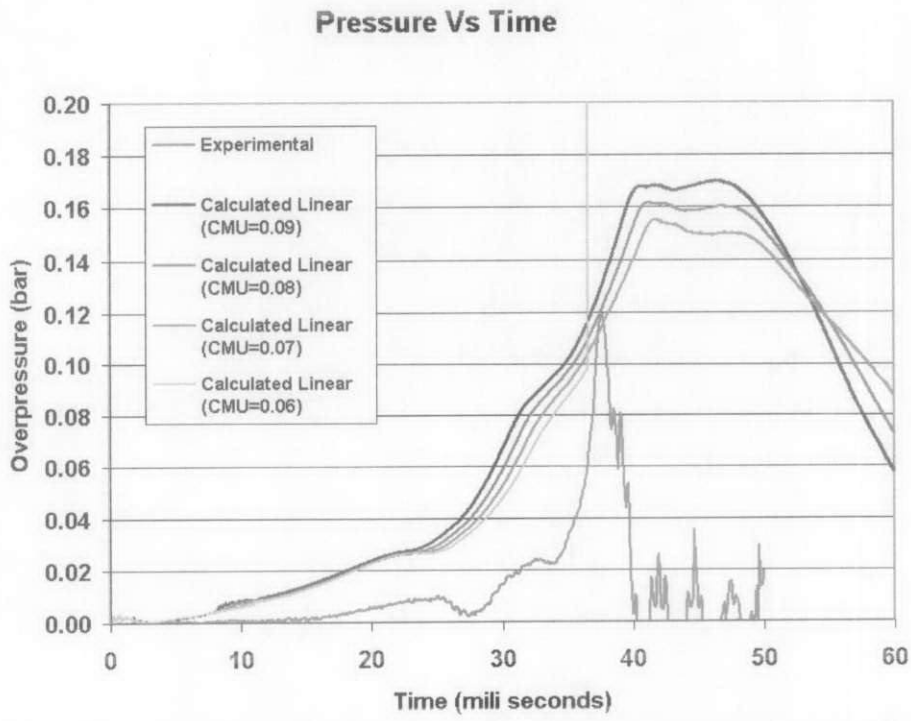


**Figure 8.7. Comparison of pressure time history of premixed methane after ignition between experimental and calculated using standard k-ε model (CMU=$C_\mu$)**

## 8.2 Applying Non-Linear k-ε Model

The Boussinesq eddy-viscosity approximation assumes that the principal axes of the Reynolds stress tensor, are coincident with those of the mean strain-rate tensor, at all points in a turbulent flow. Experimental evidence shows that flow history, effects for long distances in a turbulent flow. This is why there is a doubt about the simple linear relation (6-27).

By using the non-linear k-ε model discussed in chapter 6.3.2, the calculated results are compared with the experimental results. The comparison of the flame front propagation can be viewed in figure 8.8 and the plots of flame position and pressure in figure 8.9 and 8.10.

It is also noted that the flame front of the predicted result is much faster even at the earlier stage of the combustion, as shown by the images at 24ms. At that particular stage, the predicted results have generated flame tongues, while the experimental was just about to interact with first obstacle and experiencing flame flattening phenomena. This is again confirmed by the comparison of the flame position, showing that the calculated flame is ahead and much faster. Interestingly, now the calculated results are able to produce the recirculation behaviour just after the flame propagates through the first obstacle. This shows a very good reproduction of turbulence around this region. However it fails to simulate the burning of mixture behind the second and third obstacles. This is obvious, as there is no flame reconnection at all after the flame front passes the second obstacle.

A comparison of the pressure showed that the maximum peak pressure is now almost the same (with a difference of only 4 mbar), except that the peak of the calculated results occurred much later (around 5 s). During the earlier time, the first two peaks of pressures are higher and developed much faster for the calculated as the flame front is also quicker. The third (maximum) peak takes place at a later time due to the fact that flame position of the experimental result are already much further (at 36 ms) than the calculated (not in the plot due to the limited experimental data available), as the trend line of the experimental flame position increased very rapidly at that time.

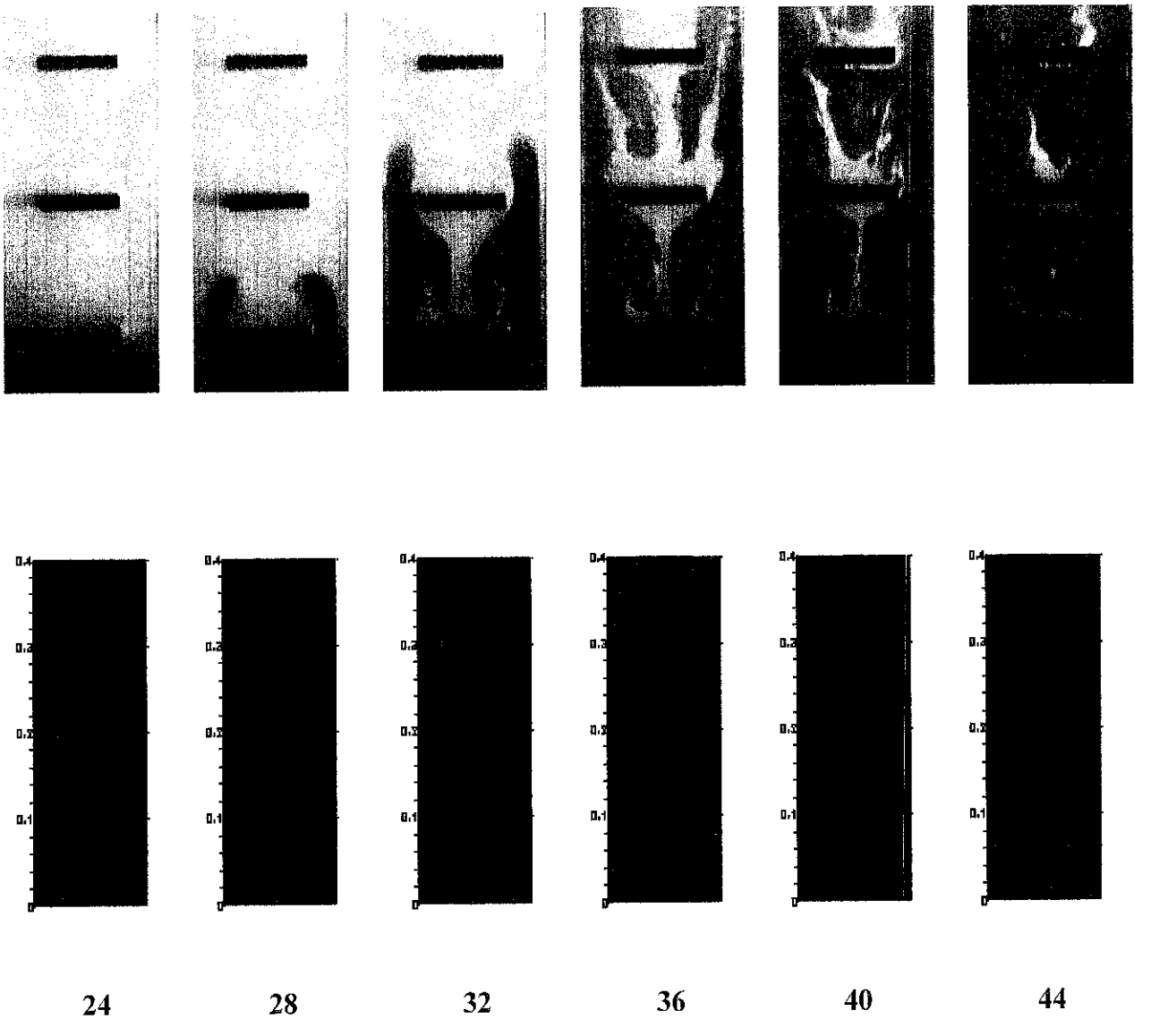


**Figure 8.8. Comparison of flame front structure of premixed methane at different times (ms) after ignition between high speed images (top) and calculated (bottom) using the non-linear k-ε model. Shown above are the images at 24 to 44 ms**

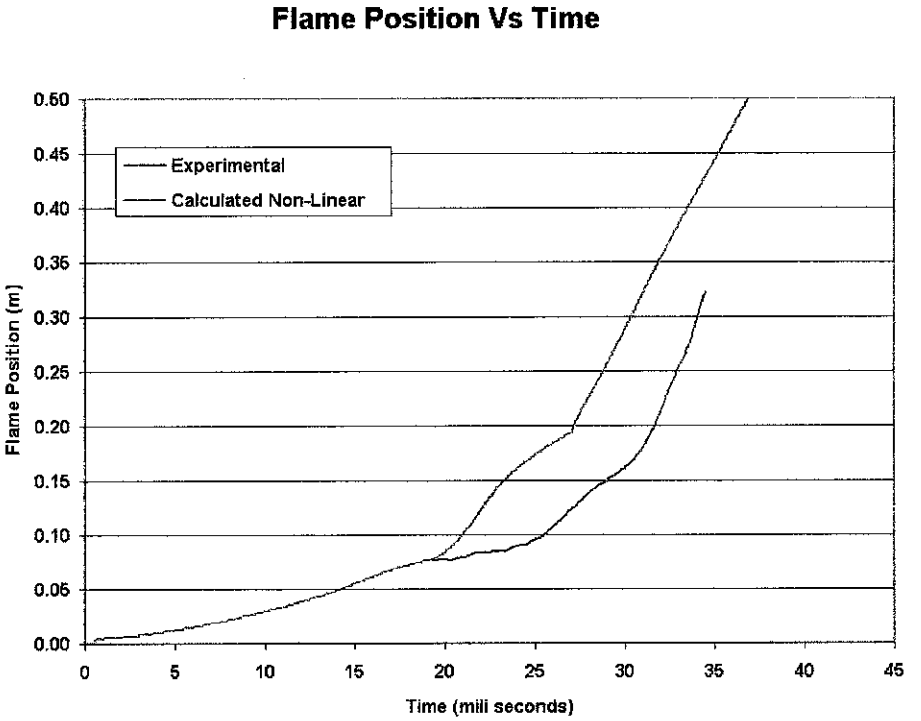


**Figure 8.9. Comparison of flame position of premixed methane after ignition between experimental and calculated using the non-linear k-ε model**

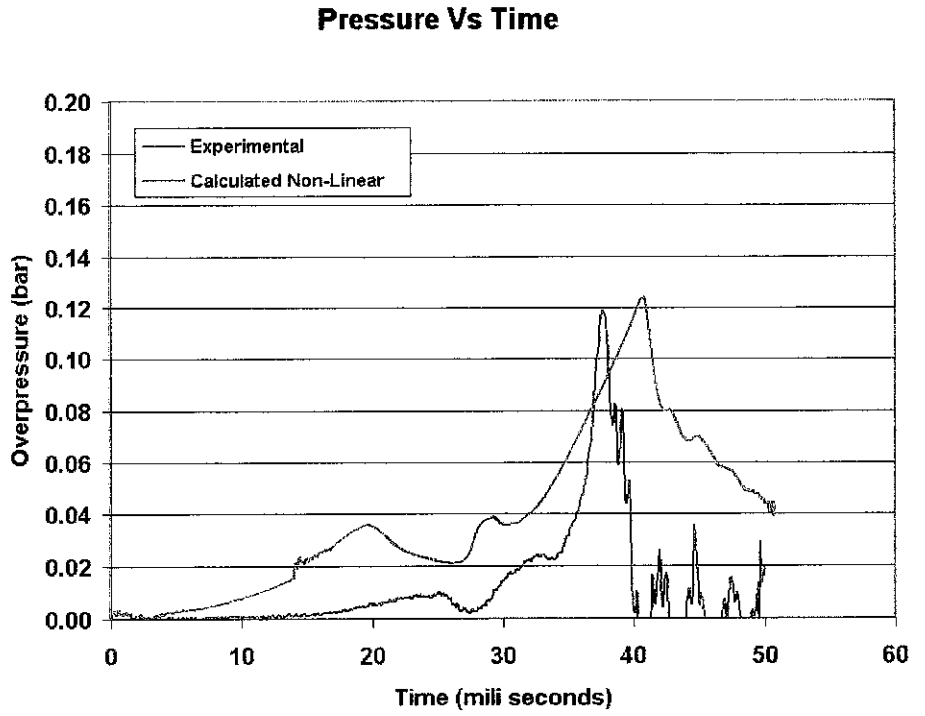


**Figure 8.10. Comparison of pressure time history of premixed methane after ignition between experimental and calculated using the non-linear k-ε model**

## 8.3 Proposed Modification on the Non-Linear k-ε Model

Since the flame front propagation simulated using non-linear k-ε model earlier does not have a good agreement with the experiment, the contour plot of $C_\mu$ for the non-linear model is generated in figure 8.11 so that the variation of $C_\mu$ across the combustion chamber at different time steps can be viewed. Hence, the build-up and drop of turbulence eddy viscosity and then the turbulence diffusion can be investigated.

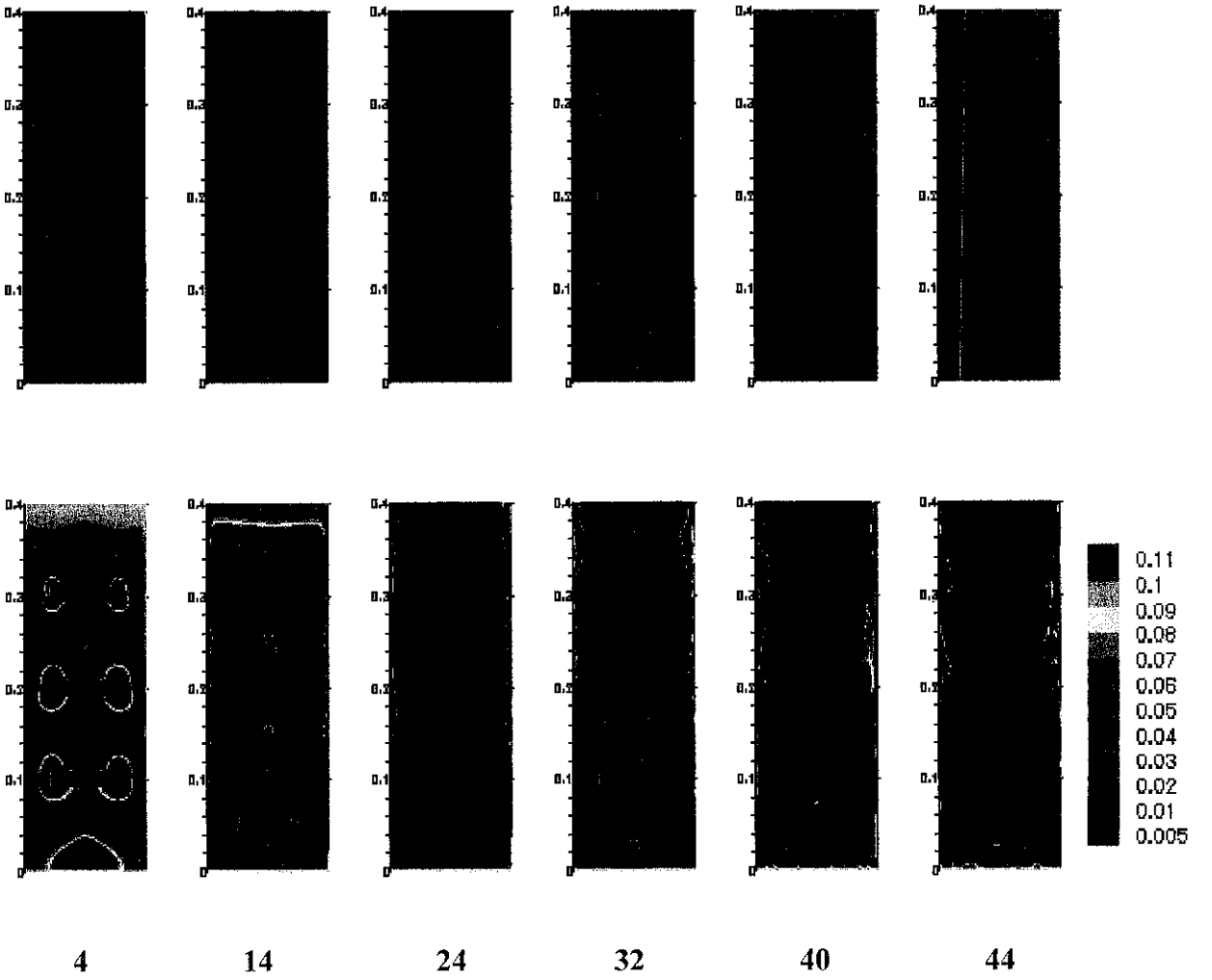


**Figure 8.11. Contour plot for Cμ at different times (ms) after ignition (bottom) for predicted result of premixed methane using the non-linear k-ε model with reference to the flame front structure (top). Shown above are the images at 4 to 44 ms**

From figure 8.11, it can be seen that during earlier time of the combustion when the flame propagation can still be assumed to be laminar (shown in the figure at 4 and 14 ms), the value of $C_\mu$ is starting from maximum almost all over the chamber (maximum $C_\mu$ value found is 0.1225) then gradually reduce. It is also noticed that after the flame interact with the first obstacle at 24 ms, the value of $C_\mu$ has dropped to a very small value almost in every section of the combustion chamber of less than 0.005 (minimum $C_\mu$ value found is $1.55\times10^{-10}$) except at the near wall regions where it is still at maximum. As the flame front propagate pass the third obstacle at 40 and 44 ms, the region of very high $C_\mu$ (near wall) behind the second obstacle has faded but after that, the intensity of $C_\mu$ has increased especially at the near wall region between first and second obstacles. This is probably the reason why we do not see the reconnection of the flame front due to the high turbulent diffusion in the near wall which make the flame propagates further and much faster without burning the trapped mixture.

To overcome the problems encounter on the flame front propagation, proposed is to put a lower limit on the value of $C_\mu$ so that it does not drop to a very small value which are very close to zero, drastically reducing the effect of the combustion diffusion (6-25). Hence, in this section the behaviour on how TRF2D reacts if a lower limit is applied by not letting the value of $C_\mu$ to drop close to zero, due to its non-linear relation ship defined by equation (6-39), is studied.

Starting by limiting the value of $C_\mu$ to be not smaller than 0.01 ($C_\mu \geq 0.01$), the calculated results is then produced. From the comparison of the flame propagation between the experimental and the calculated (also included the original non-linear model) in figure 8.12, the problem faced on the trapped mixture between obstacles seems to be improving. This is visible at 36 ms onwards. It is also noted that the flame front propagation is slower than the non-linear model simulated earlier, showing a much better agreement with the experimental. Hence, another two runs with a much higher limit on the $C_\mu$ of greater than 0.02 and 0.03 are simulated to see the effect of this variation.

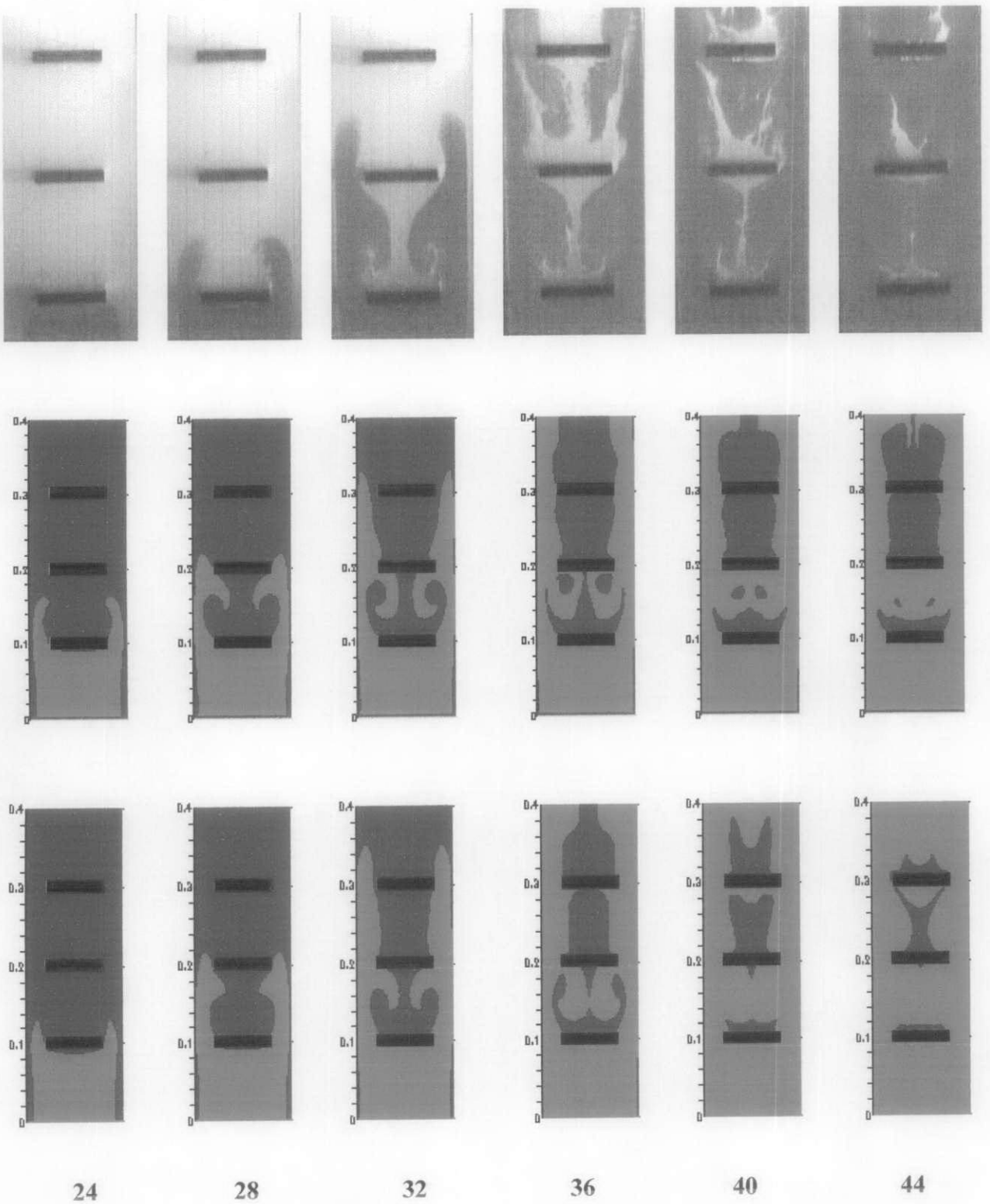


**Figure 8.12. Comparison of flame front structure of premixed methane at different times (ms) after ignition between high speed images (top), calculated using the non-linear k-ε model (middle) and calculated using the non-linear k-ε model with limitation on $C_\mu$ (bottom - $C_\mu \geq 0.01$). Shown above are the images at 24 to 44ms**

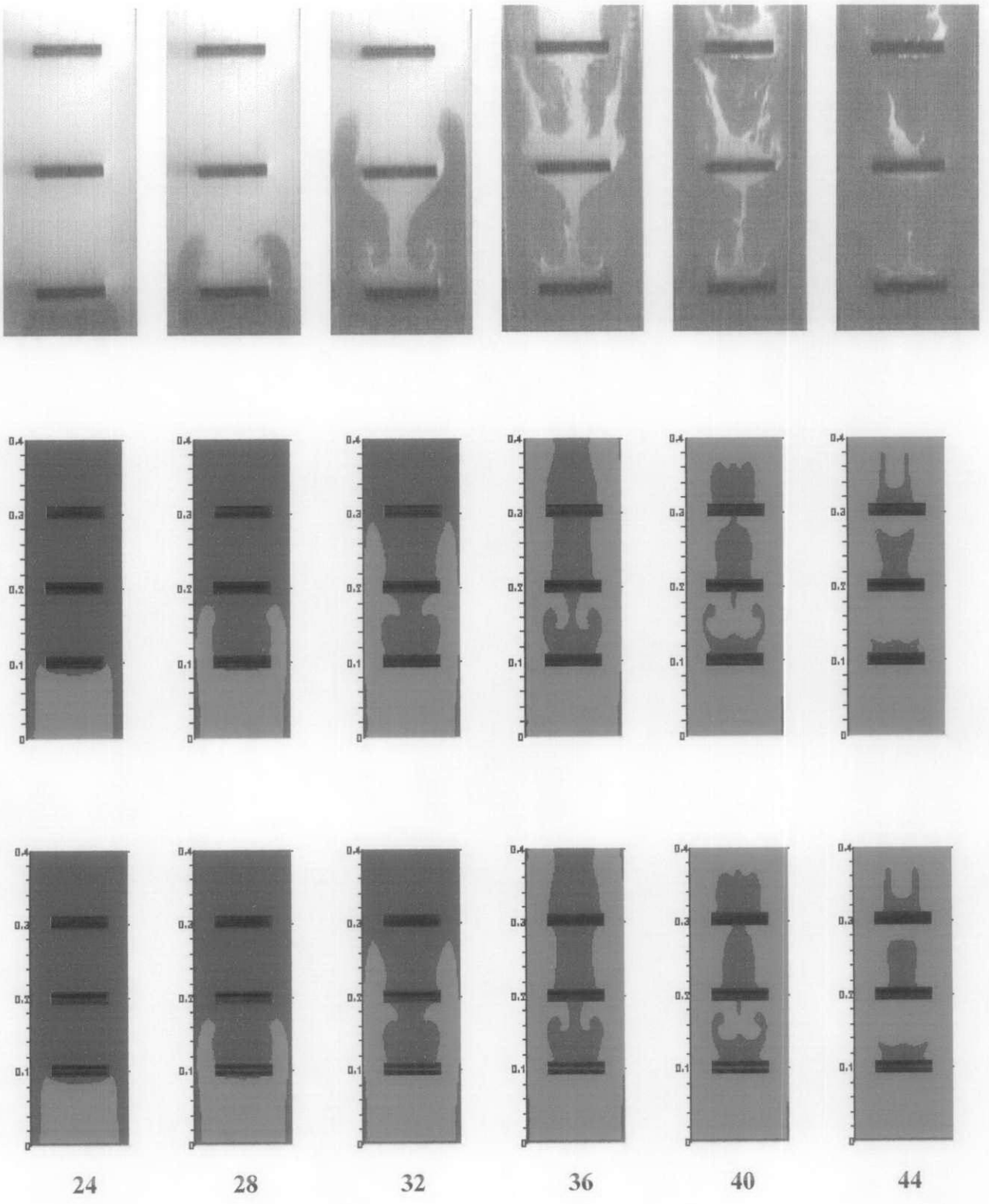


**Figure 8.13. Comparison of flame front structure of premixed methane at different times (ms) after ignition between high speed images (top), calculated using the non-linear k-e model with limitation on $C_\mu$ (middle - $C_\mu \geq 0.02$) and calculated using the non-linear k-ε model with limitation on $C_\mu$ (bottom - $C_\mu \geq 0.03$). Shown above are the images at 24 to 44 ms**

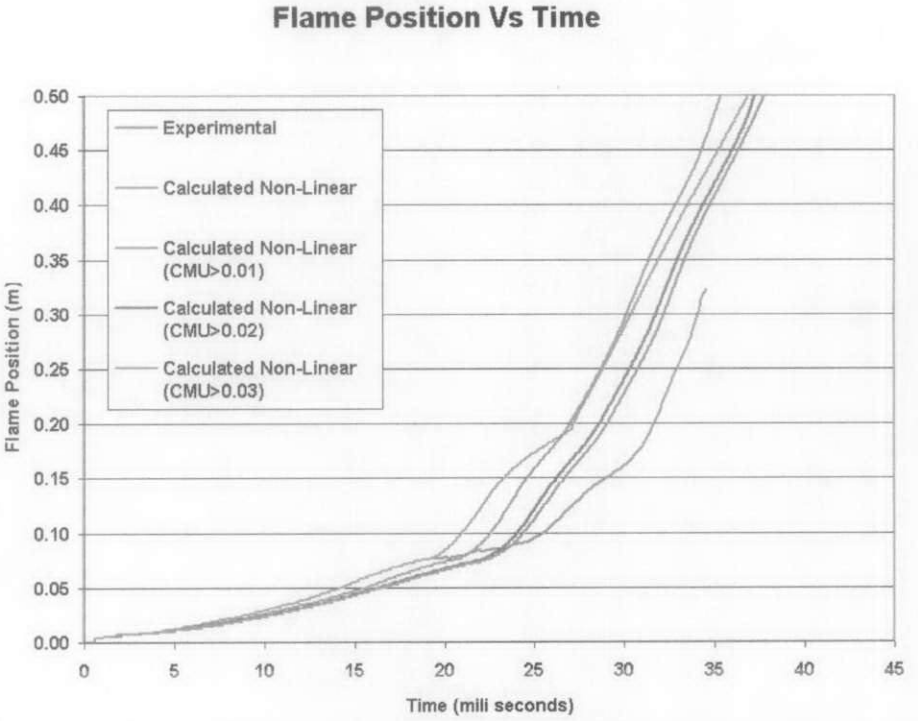


**Figure 8.14. Comparison of flame position of premixed methane after ignition between experimental and calculated using non-linear k-ε model (CMU=$C_\mu$)**

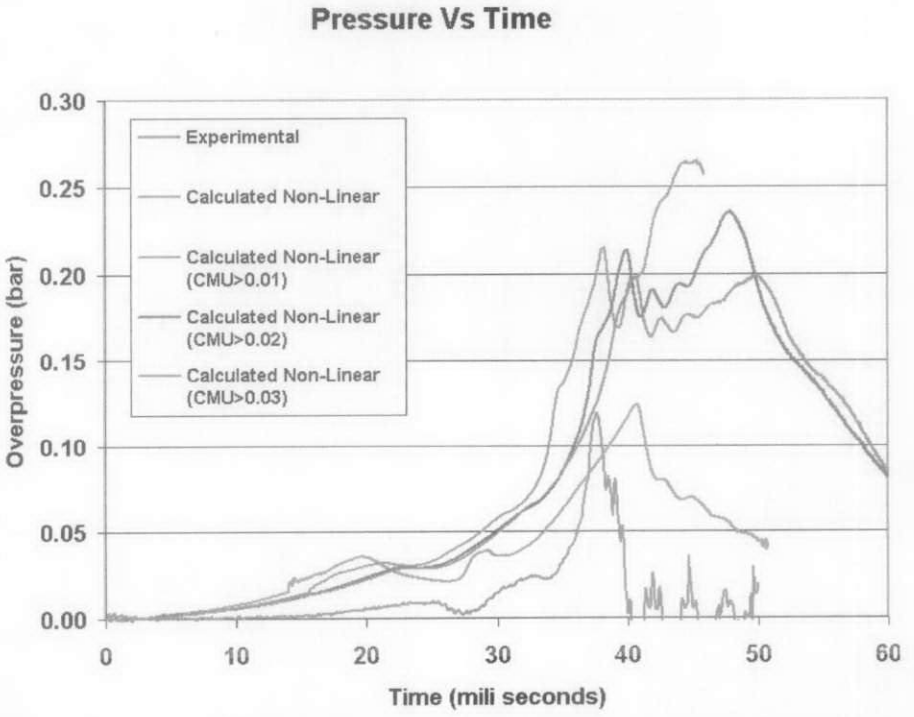


**Figure 8.15. Comparison of pressure time history of premixed methane after ignition between experimental and calculated using non-linear k-ε model (CMU=$C_\mu$)**

Figure 8.13, shows that as the limit of $C_\mu$ is increased, the flame front propagation gets slower and much better than previous. However, there is also a down effect noticed. It seems that by increasing the limit of $C_\mu$ from 0.01 to 0.02 and 0.03, the effect of high turbulence between obstacles is reduced, as can be seen from 32 ms onwards. It is observed that between the first and second obstacles the recirculation effects are less and the burn rate of trapped mixture also gets slower. It is also noticed, between the second and third obstacles, the amount of trapped mixture burned is also less.

In general, it seems that for the flame propagation, reducing the limit on $C_\mu$ has the effect of improving the flame propagation at earlier stage of the combustion. This can be confirmed from the plot of flame position on figure 8.14, where the flame position of the calculated results are getting closer to the experimental as the limit are increased. However, at later time of the combustion (after the interaction with the obstacles), increasing the limit has the effect of reducing the levels of turbulence between obstacles, which is not good.

From the pressure point of view (figure 8.15), putting the limit on $C_\mu$ make the predictions of the pressure less accurate than the original non-linear k-ε model. This increase is obvious, where at $C_\mu \geq 0.01$, the maximum peak pressure occurs during the blow-out phase and what should be the maximum peak has also increased by 90 mbar. However, increasing the limit does have an effect of improving the pressure peak. By using limit of $C_\mu \geq 0.03$, the maximum peak formed where it should be at around 40 ms. It is also noticed that the trend of the curve are getting closer to the simulated results using a standard k-ε model.

Investigation of applying an upper limit of $C_\mu$ to be less or equal than 0.1 has also been investigated. The results (although not shown) indicates almost no improvement at all. This might be due to the problem associated are solely due to the generated value of $C_\mu$ become close to zero, hence greatly affected the predicted results by reducing the diffusion of the combustion.

## 8.4 Fuel Mixture Variation

As been discussed in Chapter 6.1, the code used (TRF2D) takes account the effect of chemical kinetics. In this section, the capability of TRF2D is going to be tested when using different type of mixture. Propane and Ethylene are selected to be the mixture simulated in this test. In the code, different fuel mixtures are set by its chemical reactance or compound and appropriate laminar flame speed.

The variation of laminar-flame speed with fuel-oxidant ratio is governed predominantly by the variation of the temperature with the mixture ratio. For hydrocarbon fuels, the peak of the flame speed occurs at stoichiometric or slightly fuel-rich mixtures (for simplicity, the studies are only done at stoichiometric – in the region of maximum flame speed). Some typical results, on flame speeds as a function of fuel volume percentage in air, are shown in figure 8.16.

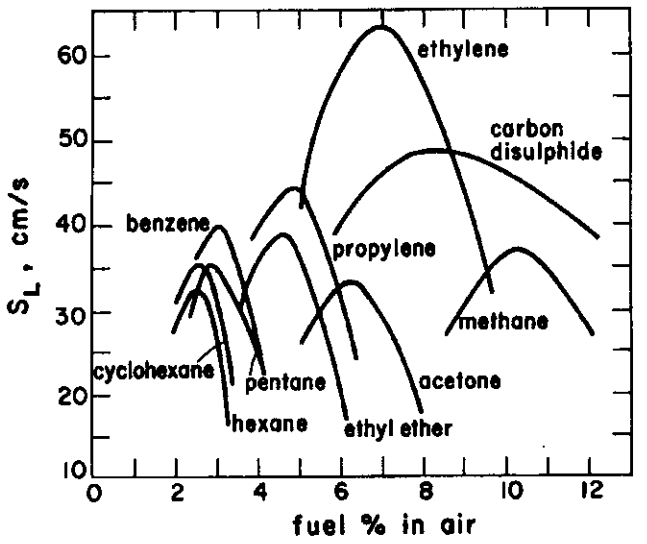


**Figure 8.16. The variation of flame speed with mixture ratio (after Kanury)**

It is generally acceptable to assume that a mixture with maximum flame temperature is also a mixture with maximum flame speed. In very lean or very rich mixtures, it is impossible to propagate a flame because there is too little fuel or oxidant to maintain a steady deflagration wave. Thus, there exist upper and lower flammability limits.

Attempts have been made to correlate the flame speed with the fuel structure. Reynolds has found that as the fuel molecular weight increases, the range of flammability becomes narrower (also shown in figure 8.16).

The difference in laminar speed for fuels containing different number of carbon atoms is mainly due to the changes in thermal diffusivity, which is a function of the fuel molecular weight. Also the reactivity of the fuel may affect the flame velocity drastically (Kuo, 1986).

There are many experimental results that give the laminar flame speed of different fuel-cited in many books and papers. Table 8 below shows the value of laminar flame speed chosen for the simulation (Turns, 1996).

**Table 8. Referenced flame speed**

| Fuel | Formula | Laminar Flame Speed ($ms^{-1}$) |
|---|---|---|
| **Methane** | $CH_4$ | 0.41 |
| **Propane** | $C_3H_8$ | 0.44 |
| **Ethylene** | $C_2H_4$ | 0.67 |

Figure 8.17, demonstrate the flame propagation of the Methane, Propane and Ethylene, while figure 8.18 and 8.19 shows its flame position and pressure time history. As been expected, the results show that the flame front propagation gets faster and faster starting from methane, propane and then ethylene. As observed from the fastest burning mixture (ethylene), the burn rate and the flame front propagation is much faster. This is displayed by the fully burned of mixture at 38 ms (shown in the figure at a later time of 40 ms) due to the big difference in the laminar flame speed. This again is confirmed from the flame position plots. The pressure plots also shows that, if a much faster burn rate of fuel is chosen, the pressure peaked much faster and higher. Eventhough there are no experimental data available for propane and ethylene, these are the sort of behaviour wanted from the code. This shows that the code follows the trends expected to simulate different fuel mixture by changing the required parameter.

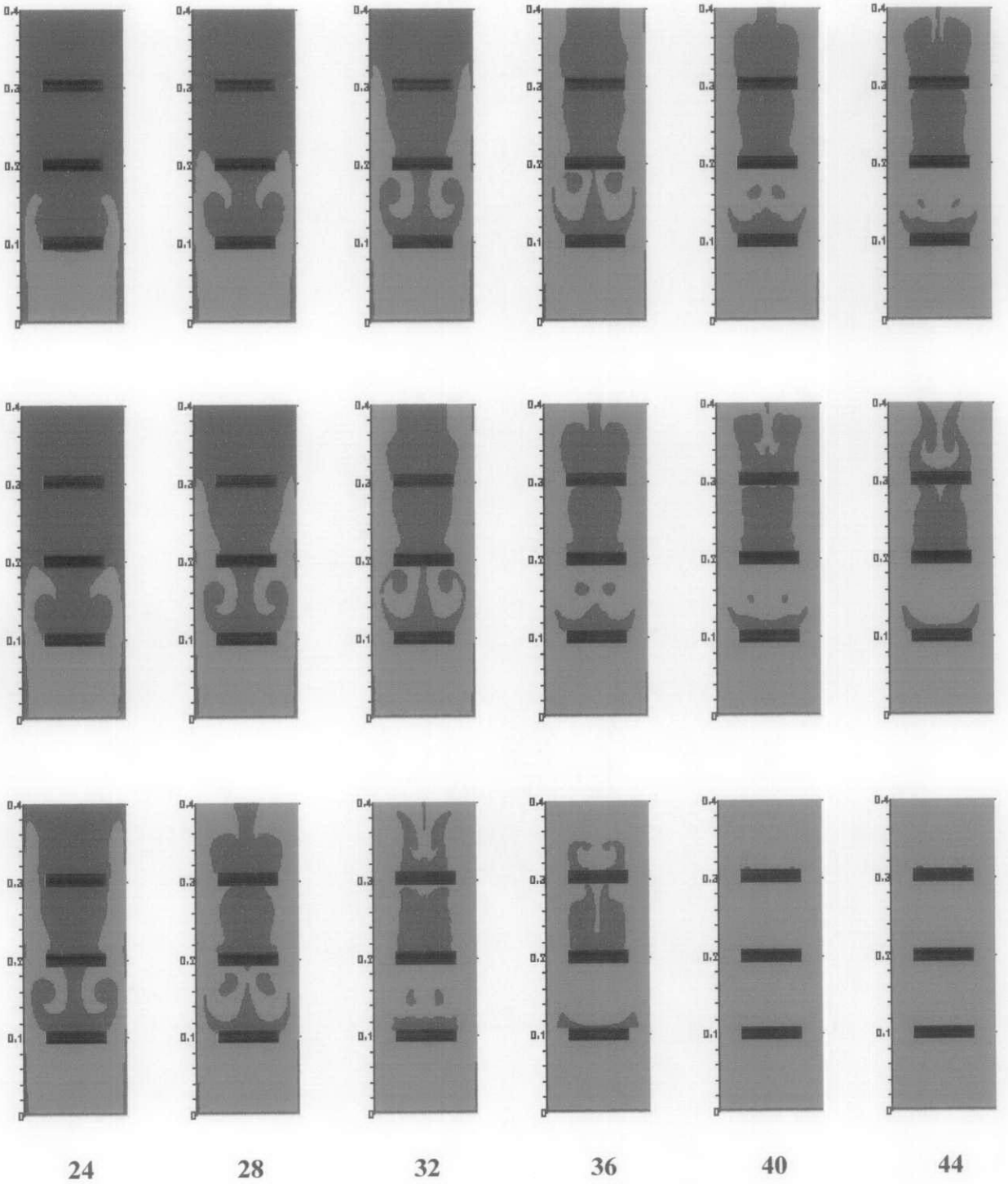


**Figure8.17. Comparison of calculated flame front structure using non-linear k-ε model of premixed methane (top), propane (middle) and ethylene (bottom) at different times (ms) after ignition. Shown above are the images at 24 to 44 ms**

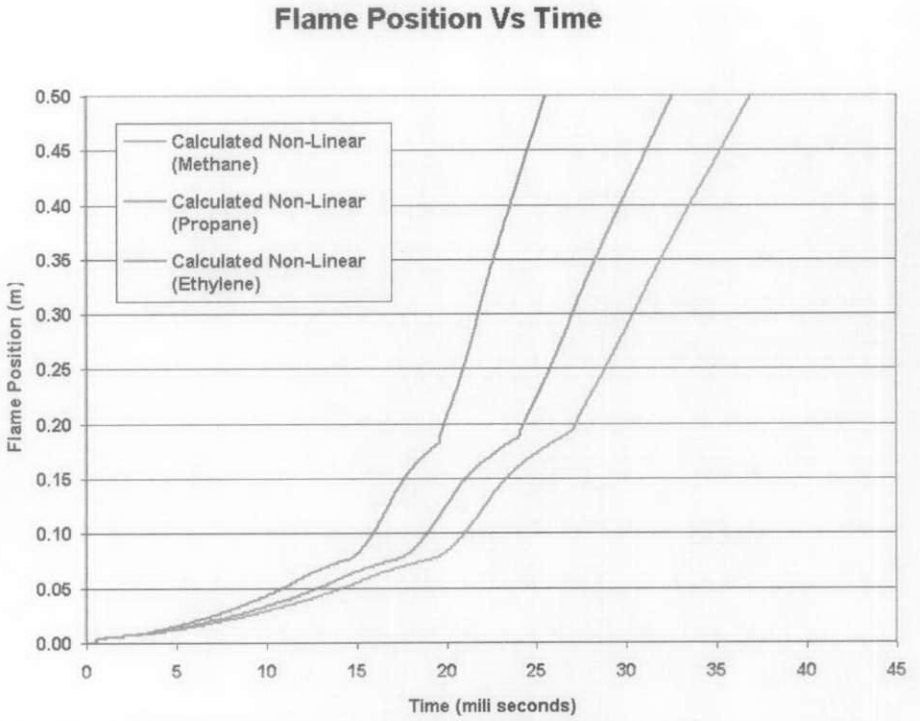


**Figure 8.18. Comparison of flame position of premixed methane, propane and ethylene after ignition between experimental and calculated using the standard k-ε model**

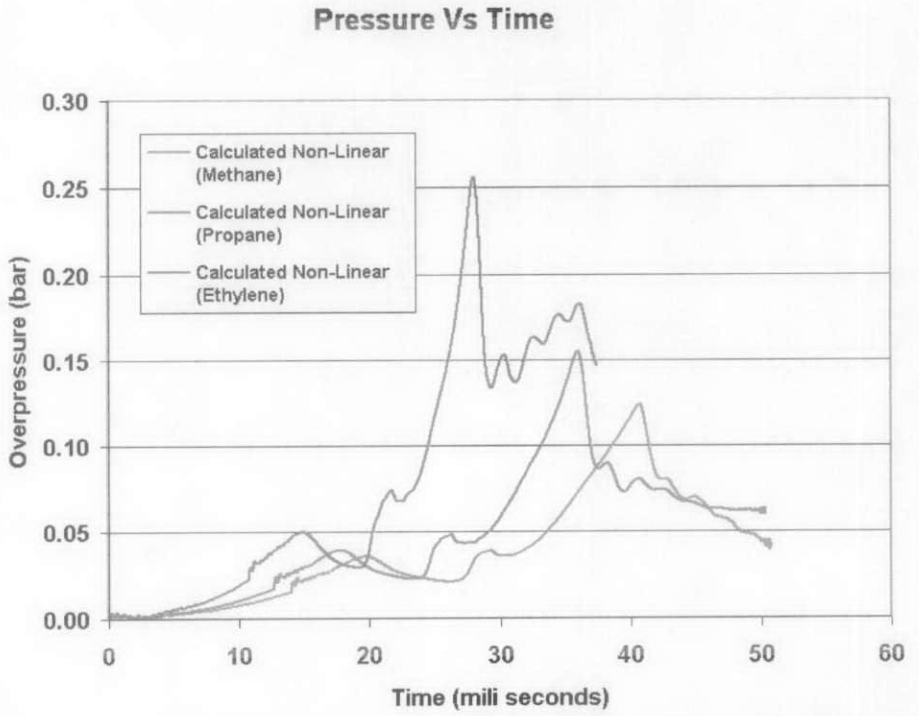


**Figure 8.19. Comparison of pressure time history of premixed methane, propane and ethylene after ignition between experimental and calculated using the standard k-ε model**

## 8.5 Combustion Regimes of the Approach

It is one of the interests to know whether the approach used by TRF2D is good for the studies of SI engine as been discussed in chapter 4. Therefore, it is important to determine the regimes of combustion of the calculated results. By plotting the turbulence Reynolds number on the horizontal axis and an overall turbulence Damkohler number (the ratio of a turbulence time to a chemical time) on the vertical axis, it is noted that the approach used is suitable for the studies of the SI engine. This is shown in Appendix (Averaged plot of Combustion Regimes as in figure 4.1, chapter 4), as all the averaged calculated results (shown by a circles plot) lies in the SI engine combustion regime for all the simulated results.

# 9 Conclusion and Future Work Recommendations

Numerical work has been done to assess the performance of the mathematical model using various combustion and turbulence models with different configurations. A RANS code called TRF2D was used in simulating the test case of the experiment being done at Loughborough University. The test case does provide challenging situations, which demonstrate the various problems faced when simulating combustion in spark ignition engine.

The standard turbulence model failed to reproduce the recirculation phenomena that occurred behind the obstacles. This is due to the anistropy assumptions that was unable to demonstrate the complex nature of the vortices generated by the recirculating flow. There is also an over prediction of pressure took place. By reducing the constant $C_\mu$ used in the model, it is apparently a slightly better representation of the experimental. However, there is a minimum limit where this can be applied. Furthermore there were still no recirculations phenomena displayed. It can be said that the standard linear k-ε model is often capable of providing good results, but it is incapable of predicting swirling flows, the effects of strong streamline curvature and flows with boundary-layer separation, just to mention some of its limitations.

By using the non-linear turbulence model, it allows an improvement of the flame front at the downstream location, especially between the first and the second obstacles, where the axial and swirl velocities agree well with experimental images shown by the recirculation and turning of the flame front. Meanwhile further upstream the prediction accuracy decreases and the velocities are in general too high. Nevertheless, the predicted pressure time history shows a close correlation with experimental results, which turn out to be the best results for pressure.

Applying minimum limit to the constant $C_\mu$ on the non-linear turbulence model improves the flame front at the upstream location but produced a poorer result for the pressure time history even if compared to the standard turbulence model. Increasing

this minimum limit of $C_\mu$ helps to improve the pressure fluctuation but with a loss on the flame front results. However, the loss is not as significant as the improvement gained on the pressure. The highest minimum limit applied ($C_\mu \geq 0.03$) seems to be the best result as it takes the trade off between the flame front and the pressure and performed in the middle for both, hence producing the best result overall.

During the simulation of using different premixed mixtures, a faster flame speed and a much higher calculated pressure peaks were found for faster burning fuels. This proves that the code is able to indicate the rate of heat release experienced in the combusting premixed fuel mixture. Eventhough validation of using propane and ethylene was not available, the results are as what to be expected. This shows that the code was able to predict the expected trends when applying different type of fuels.

As been displayed by the Combustion Regime plots of the calculated results, where within all the regions in the combustion chamber, the Damkohler number that is plotted against the Reynolds number falls within the region of SI engine reaction. These shows that the code used will be an excellent simulator for SI engine combustion.

For future work, since only stoichiometric mixture were considered in this report, the study of using lean and rich mixture should be investigated and validated with experimental results. This is important as the stoichiometries of mixture used in an SI engine varies and normally operates at a slightly lean mixture. Hence, additional research should be carried out particularly on the accuracy of the code predicting at slightly lean mixture. This is because most of the research to improve the design of an SI engine falls within this region, as lean burn improves its fuel consumption and produce lower emissions, which is an important issue for the improvement of engine performance.

An extension of study and validation of ignition at elevated pressure might also be essential since the simulations are only done where the mixture is at atmospheric pressure and this are not the case for an SI engine. Then research should be carried out to extend the combustion model to a full 3D calculations.

Simulation of real combustion chamber geometry of an engine should be studied. The investigation on how TRF2D could be applied to simulate the real combustion condition inside an SI engine also needs to be researched further. For instance, the need to introduce a higher level of turbulence before igniting the mixture, as it exists inside the combustion chamber of an SI engine due to the intake process. Then the research could further touch on how to create the same pressure during ignition since the premixed fuel is ignited during compression and also the effect of expansion has on the pressure time history.

Means to take account the intermittency phenomena between fresh and burned gases in turbulent premixed flame have to be further explored if a much real condition of SI engine is to be simulated. This is due to the fact that during the exhaust process, not all the burned mixture is released to the atmosphere, a small amount might be trapped and mixed with a fresh premixed mixture during the intake. This capability will also extend the use of the code to study the effect of exhaust gas recirculation (EGR).

An interaction of TRF2D with other code should also be tested. For example, the interactions with a spray code to produce and simulate the atomisation of fuel and producing a premixed mixture in the combustion chamber. This will then produce a code which will be able to simulate a direct injection condition, which is a very popular study of combustion nowadays and with the advancement of the optical diagnostics the experimental data is widely available for validation purposes.

# Appendix

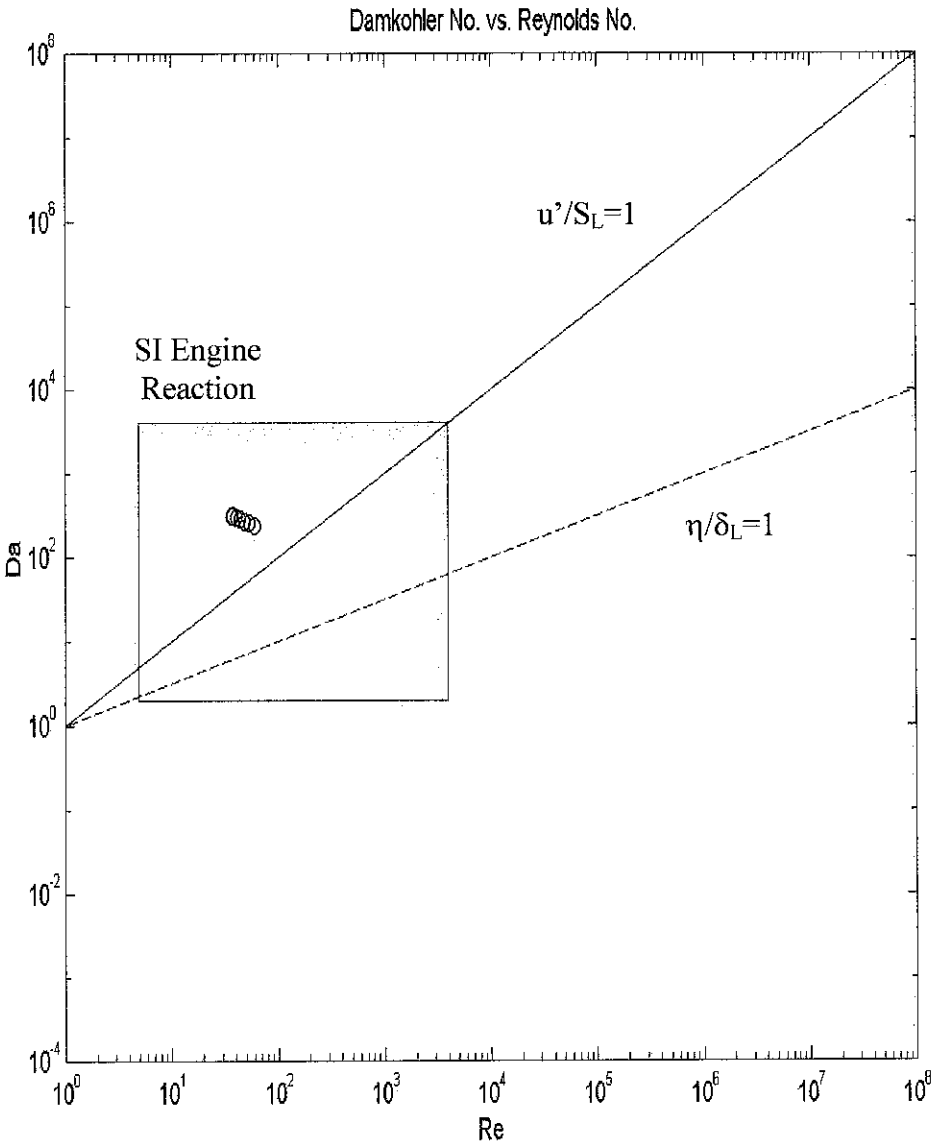


**Calculated Regimes of Turbulent Combustion of premixed methane at stoichiometric using the standard k-ε turbulence model. The red rectangle identifies the regime of SI engine operating conditions**

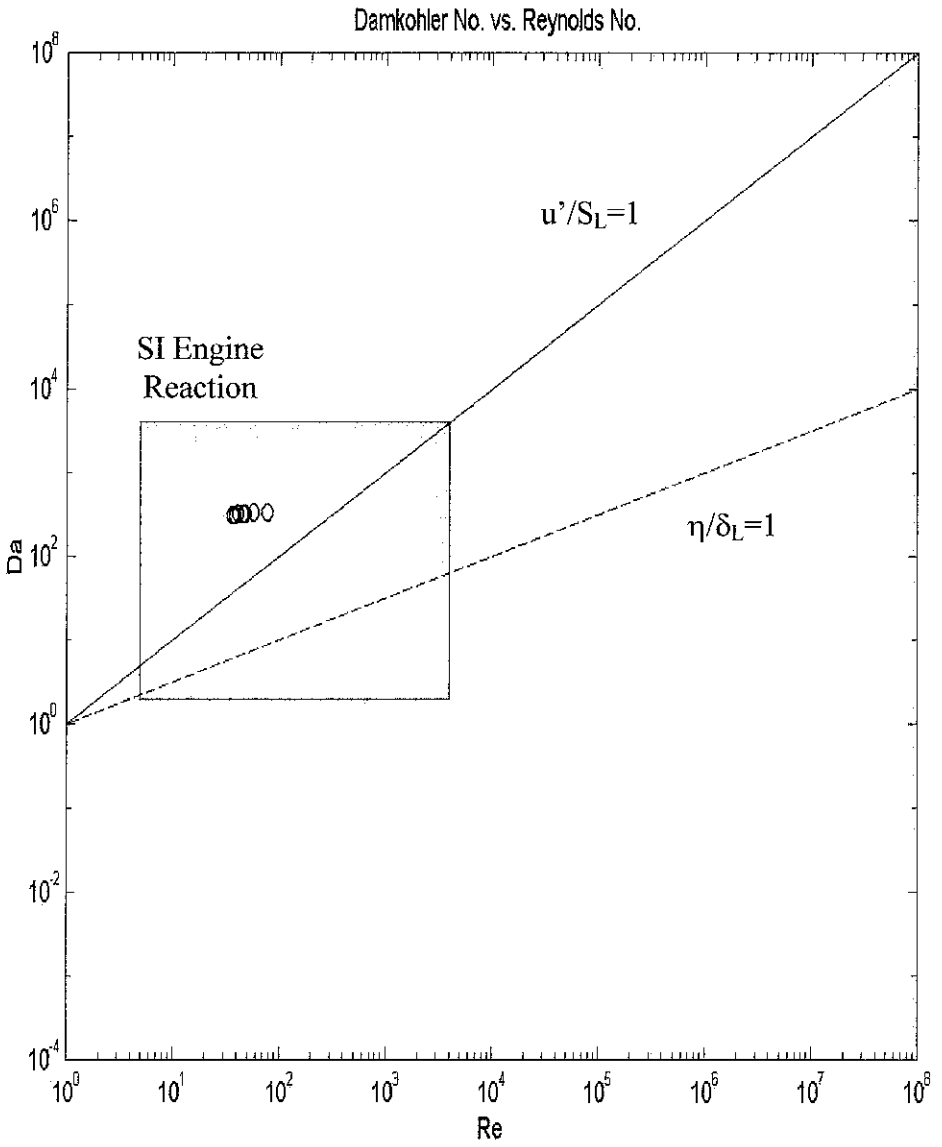


**Calculated Regimes of Turbulent Combustion of premixed methane at stoichiometric using the non-linear k-ε turbulence model. The red rectangle identifies the regime of SI engine operating conditions**

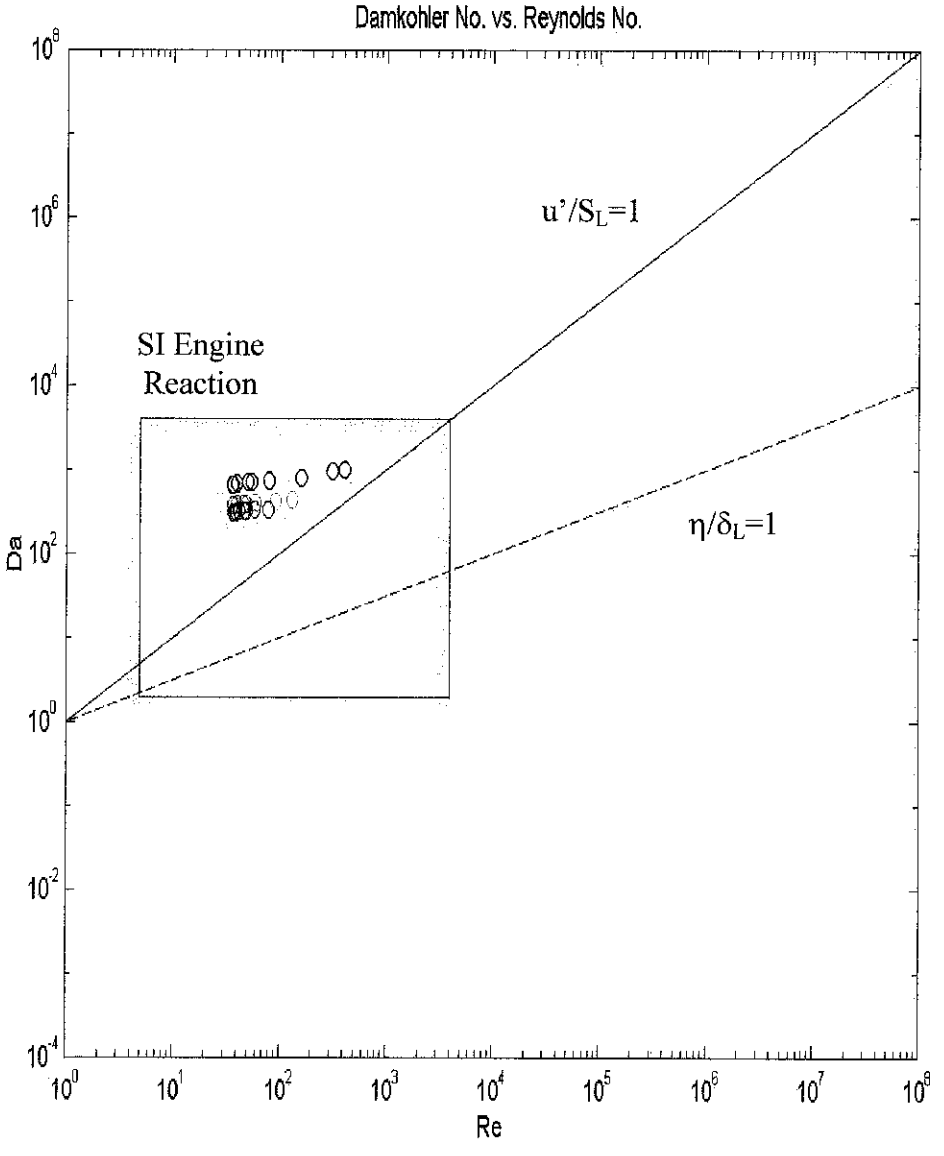


**Calculated Regimes of Turbulent Combustion of premixed methane (black circles), propane (green circles) and ethylene (blue circles) at stoichiometric using the non-linear k-ε turbulence model. The red rectangle identifies the regime of SI engine operating conditions**

# References


1. Abdel-Gayed, R. G., Bradely D. and Lawes, M., "*Turbulent burning velocities: a general correlation in terms of straining rates*", Proc. R. Soc. London, Ser. A, 414, pg. 389, 1987.

2. Abdel-Gayed, R. G., Bradley, D., Lung, F. K. K., "*Combustion Regimes and the Straining of Turbulent Premixed Flames*", Combustion and Flame 76: 213-218, 1989.

3. Abraham, J., Williams, F. A., Bracco, F. V., "*A Discussion of Turbulent Flame Structure in Premixed Charges*", SAE Paper 850345, 1985.

4. Borghi, R., "*Recent Advances in the Aerospace Sciences*", Plenum Press, New York, 1985.

5. Bray, K. N. C., "*Studies of turbulent burning velocity*", Proc. R. Soc. London, Ser. A, 431, pg. 315, 1990.

6. Bray, K. N. C,. "*The Challenge of Turbulent Combustion*", 26th Symposium (Int.) on Combustion, The Combustion Institute, Pittsburgh, pg. 1–26. (1996).

7. Ching-Jen Chen and Shenq-Yuh Jaw, " Fundamental of Turbulence Modelling", Taylor and Francis, 1998.

8. Craft, T. J., Launder, B. E. and Suga, K., "*Extending the applicability of eddy viscosity models through the use of deformation invariance and non-linear elements*", 5th Int. Sump. Of Refined Flow Modelling and Turbulence Measurements, 1993.

9. Duclos, J. M., Veynate, D. and Poinsot T., "*A comparison of flamelet models for premixed turbulent combustion*", Combust. Flame, 95, pg.101, 1993.

10. Glassman I., "*Combustion*", Academic Press, Inc, 1987.

11. Ibrahim, S. S., Hargrave, G. K., Williams T. C., "*Experimental Investigation of Flame/Solid Interactions in Turbulent Premixed Combustion*", International Journal of Experimental Heat Transfer, Thermodynamics and Fluid Mechanics, 2001.

12. Issa, R. S., "*Solution of the implicitly discretised fluid flow equations by operator splitting*", J. Comp. Phys., 62, pg. 40-65, 1986.

13. Jarvis, S., Hargrave, G. K. and Ibrahim, S. S., "*An experimental investigation of flame deflagration over single and multiple solid obstacles*", 18th International Colloquium on the Dynamic of Explosions and Reactive Systems, Seattle, 2001.

14. Kanury, A. M., "*Introduction to Combustion Phenomena*", Chapter 8, Gordon and Breach, New York, 1975.

15. Kundu, P. K., "*Fluid Mechanics*", Academic Press, London, 1990.

16. Kuo, K. K., "*Principles of Combustion*", John Wiley, 1986.

17. Kuo, N. S., Lin, Y. C. and Lin, C. A., "*Computations of Recirculating Flows with Non-linear Eddy Viscosity Models*", 3rd International Symposium on Turbulence, Heat and Mass Transfer, pg. 397, 2000.

18. Launder, B. E., Spalding, D. B., "*Mathematical Models of Turbulence*", Academic Press, London and New York, 1972.

19. Libby P. A., Williams F. A., "*Turbulent Reacting Flows*", Springer-Verlag, Berlin, 1980.

20. Libby, P. A. and Williams, F. A., "*Turbulent Reacting Flows*", Academic Press, London, 1994.

21. Linan A., Williams F. A., "*Fundamental Aspects of Combustion*", Oxford University Press, New York, pg. 111-151, 1993.

22. Maly, R. R., "*State-of-the art and future needs in S.I. engine combustion*", in 25th Sympos. (Int.) on Combustion, pg. 111. The Combustion Institute, 1994.

23. Metghalchi, M., Keck J. C., "*Burning Velocities of air with methanol, isooctane, and indolene at high pressure and temperatures*", Combust and Flame, 48, pg. 191, 1982.

24. North, G. L and Santavicca, D. A., "*The fractal nature of premixed turbulent flames*", Combust. Sci. Technol., 72, pg. 215, 1990.

25. Patel, S. N. D. H. and Ibrahim, S. S., "*Burning velocities of propagating turbulent premixed flames*", Proc. of the first international symposium on turbulence and shear flow phenomena, pg. 837, 1999.

26. Patel, S. N. D. H and Ibrahim, S. S., "*Calculations of burning velocity of turbulent premixed flames using a flame surface density model*", Submitted to the Journal of Combustion Theory and Modelling, 2001.

27. Patel S. N. D. H., "*Modelling of Premixed Turbulent Propagating Flames*", Doctoral Thesis, Loughborough University, 2001.

28. Peters, N., "*Laminar Flamelet Concepts in Turbulent Combustion*", Invited Lecture, 21st Symposium (International) on Combustion, The Combustion Institute, Pittsburgh, pg. 1231-1250, 1986.

29. Peters N., "*Turbulent Combustion*", Cambridge University Press, Cambridge, 2000.

30. Poinsot, T. and Veynante, D., "*Theoretical and Numerical Combustion*", R. T. Edwards, Inc., 2001.

31. Spalart, P. R., "*Strategies for turbulence modelling and simulations*", International Journal of Heat and Fluid Flow, vol. 21, pg. 252, 2000.

32. Strahle, W. C., "*Duality, dilatation, diffusion and dissipation in reacting turbulent flows*", in 19th Sympos. (Int.) on Combustion, p. 337. The Combustion Institute, 1983.

33. Turns, S. R., "*An Introduction to Combustion*", McGraw-Hill, Singapore, 1996.

34. Warnatz, J., Mass, U. and Dibble, R.W., "*Combustion: Physical and Chemical Fundamentals; Modelling and Simulation; Experiments; Pollutant Formation*", Springer, 1996.

35. Williams F. A., "*Combustion Theory*", Addison-Wesley, 1985.

36. Williams F. A., "*Some Recent Studies in Turbulent Combustion*", Smart Control of Turbulent Combustion, 2001.